UNIVERSITÀ
DEGLI STUDI
DI PADOVA

Sede Amministrativa: Università degli Studi di Padova

Dipartimento di Scienze Biomediche

SCUOLA DI DOTTORATO DI RICERCA IN BIOSCIENZE E BIOTECNOLOGIE
INDIRIZZO IN NEUROBIOLOGIA
CICLO XXIV

MECHANISMS OF INDUCTION AND PROPAGATION OF CORTICAL SPREADING DEPRESSION IN MOUSE BRAIN SLICES

Direttore della Scuola: Ch.mo Prof. Giuseppe Zanotti
Coordinatore d'indirizzo: Ch.mo Prof. Daniela Pietrobon
Supervisore: Ch.mo Dott. Giorgio Carmignoto
Ch.mo Prof. Daniela Pietrobon

Dottorando: Andrea Urbani

INDEX

Abbreviations

ACh: acetylcholine
AMPA: (RS)-α-amino-3-hydroxy-5-methyl-4-isoxadepropionate
ATP: adenosine-5'-triphosphate
BOLD: blood oxygenation level-dependent
Ca^{2+}: calcium
$[Ca^{2+}]$: calcium concentration
CGRP: calcitonin gene-related peptide
CSD: cortical spreading depression
D-AP5: D(-)-2-amino-5-phosphonopentanoic acid
FHM1: familial hemiplegic migraine type 1
Fluo-4: Fluo-4, AM
FS: fast-spiking
GABA: γ-aminobutyric acid
GCS: gluconate cutting solution
GTP: guanosine-5'-triphosphate
H+: hydrogen
HEPES: N-2-hydroethylpiperazine-N'-2-ehanesulfonic acid
HVA: high voltage activated
K^+: potassium
$[K^+]o$: extracellular potassium concentration
KI: knock-in
LJP: liquid junction potential
LTP: long-term potentiation
LVA: low voltage activated
MA: migraine with aura
mACSF: modified artificial cerebrospinal fluid
MCS: mannitol cutting solution
NMDA: N-methyl-D-aspartate
OGB1-AM: Oregon Green® 488 BAPTA-1, AM
P: postnatal day
RQ KI: R192Q knock-in
sACSF: standard artificial cerebrospinal fluid
SR101: sulforhodamine 101
WT: wild-type
ω-AgaIVA: ω-agatoxin IVA
ω-CgTxGVIA: ω-conotoxin GVIA

Riassunto

L'emicrania è un disturbo neurologico comune ed altamente invalidante che colpisce più del 10% della popolazione in generale; nel 30% dei pazienti affetti da emicrania, la fase del dolore è preceduta da sintomi neurologici transienti definiti nel complesso "aura emicranica". L'emicrania emiplegica familiare di tipo 1 (FHM1) è un forma autosomica dominante di emicrania con aura rara ma molto grave; l'FHM1 è considerata un buon modello per lo studio dell'emicrania: gli attacchi tipici di FHM1, infatti, ricapitolano molto quelli della normale emicrania con aura, tuttavia durante l'aura si presentano sintomi come debolezza motoria o paralisi, spesso ma non sempre unilaterale. L'FHM1 è dovuta a mutazioni nel gene CACNA1A che codifica la subunità α_1 formante il poro dei canali Ca^{2+} neuronali voltaggio dipendenti $Ca_V2.1$, chiamati anche canali per il calcio di tipo P/Q.

Le mutazioni FHM1 producono un guadagno di funzione dei canali ricombinanti umani $Ca_V2.1$; tale guadagno di funzione è principalmente dovuto allo spostamento della curva di attivazione del canale verso valori di potenziale più negativi e all'aumento della probabilità di apertura e dell'influsso di Ca^{2+} a livello di singolo canale in un ampio intervallo di potenziali vicini alla soglia di attivazione del canale (Hans et al., 1999; Tottene et al., 2002, 2005).

Studi *in vivo* (van den Maagdenberg et al., 2004) ed *in vitro* (Tottene et al., 2009) hanno dimostrato come topi knock-in (KI) per la mutazione umana FHM1 R192Q presentino una facilitazione nell'induzione sperimentale della *cortical spreading depression*, il fenomeno neurologico alla base dell'aura emicranica e possibile evento innescante il tipico mal di testa caratterizzante l'emicrania. Dal punto di vista elettrico la CSD è un'onda di forte depolarizzazione neuronale e gliale, che si propaga lentamente attraverso la corteccia cerebrale ed è seguita da una lunga fase di soppressione neurale.

Recentemente Tottene e colleghi (2009) hanno dimostrato un aumento nella trasmissione sinaptica eccitatatoria corticale dei topi FHM1 R192Q; tale aumento è dovuto all'aumentato influsso di Ca2+ evocato da potenziali d'azione attraverso i canali $Ca_V2.1$ ed al conseguente aumento nella probabilità di rilascio del neurotrasmettitore glutammato alle sinapsi piramidali di questi topi. Attraverso l'impiego di un modello *in vitro*, Tottene e colleghi hanno, inoltre, dimostrato il rapporto di causalità tra l'aumentato rilascio di glutammato dai neuroni piramidali e la facilitazione nell'induzione della CSD tramite brevi applicazioni pressorie di KCl a concentrazioni elevate in fettine di cervello da questi topi. Tali evidenze supportano l'ipotesi di un ruolo chiave dei canali $Ca_V2.1$ nei meccanismi di induzione e propagazione della CSD.

La prima parte del mio progetto di dottorato ha avuto come scopo fondamentale l'approfondimento delle conoscenze riguardo i meccanismi che sottendono induzione e la propagazione della CSD; in particolare il mio interesse si è principalmente soffermato sul ruolo dei canali del calcio voltaggio-dipendenti e dei recettori NMDA. I risultati ottenuti sono stati pubblicati (Tottene et al., 2001, pdf allegato nel capitolo 3). Per conseguire gli scopi prefissi abbiamo impiegato il modello *in vitro* già in precedenza adottato da Tottene e colleghi (2009) ed abbiamo misurato la soglia di induzione della CSD e la velocità di propagazione della stessa in fettine corticali di topo *wild-type* (WT) prima e dopo l'applicazione di vari inibitori selettivi dei canali d'interesse. La durata del primo impulso in grado di indurre una CSD veniva considerata la soglia di induzione della stessa, mentre la velocità di propagazione della CSD coincideva con la velocità di propagazione dei cambiamenti nel segnale ottico intrinseco (IOS) associati ad essa. Il ruolo dei recettori NMDA è stato indagato mediante l'impiego di un inibitore selettivo in concentrazione saturante: D-AP5, 50 μM. In presenza di D-AP5 stimoli fino a 30 volte la soglia controllo non erano in grado di indurre una CSD. Abbiamo inoltre indagato il ruolo dei canali per il Ca^{2+} voltaggio-dipendenti di tipo P/Q, N, R ed L, usando i rispettivi inibitori specifici: ω-agatossina IVA (300 nM), ω-conotossina GVIA (1 μM), SNX-482 (250 nM) e nimodipina (50 μM). Similmente a quanto osservato in presenza di D-AP5, in presenza di ω-AgaIVA, stimoli fino a 30 volte la soglia controllo non erano in grado di indurre una CSD. Diversamente, l'applicazione di ω-CgTxGVIA o di SNX-482 provocava un lieve innalzamento della soglia (di circa il 10%) e una leggera diminuzione della velocità (di circa il 15%), suggerendo un ruolo modulatore dei canali per il calcio voltaggio-dipendenti di tipo N ed R nell'induzione e nella propagazione della CSD. Al contrario l'applicazione di nimodipina non aveva alcun effetto sulla soglia o sulla velocità della CSD. La dimostrazione che D-AP5 e ω-AgaIVA sono in grado di inibire totalmente l'induzione e la propagazione della CSD, mentre CgTxGVIA, SNX-482 e nimodipina presentano solo un lieve effetto, o nessun effetto, sono consistenti con ed avvalorano un modello di induzione e propagazione della CSD nel quale l'attivazione dei canali $Ca_V2.1$ presinaptici (e forse anche di quelli postsinaptici) e dei recettori NMDA ha un ruolo essenziale (Tottene et al., 2011).

Il ruolo dei recettori NMDA è stato ulteriormente indagato, sfruttando i topi KI FKM1 R192Q, che presentano un incrementato rilascio di glutammato da parte dei neuroni piramidali. Contrariamente a quanto riscontrato nei WT, in questi topi l'applicazione di D-PA5 non era in grado di bloccare l'induzione della CSD, ma aumentava invece significativamente la soglia (90 ± 9%) e diminuiva significativamente la velocità (47 ± 1%) rispetto al controllo. Il diverso effetto del D-AP5 riscontrato nei topi WT ed in quelli KI potrebbe suggerire che altri elementi (oltre ai recettori NMDA) potrebbero essere coinvolti nell'induzione e nella propagazione della CSD.

Registrazioni in current-clamp in prossimità del sito di eiezione del KCl, alle distanze fisse di 100 e 200 μm, hanno permesso di osservare e distinguere diverse fasi nei cambiamenti di voltaggio indotti dall'applicazione di stimoli di KCl sottosoglia e a soglia; è stato infatti possibile osservare la presenza di tre diversi picchi. Mentre i primi due picchi erano condivisi dalle depolarizzazioni sottosoglia e dalla CSD, la comparsa del terzo picco era specificamente legata all'induzione della CSD. La tecnica del patch-clamp ha permesso di descrivere nel dettaglio le diverse fasi di depolarizzazione, mostrando tuttavia l'ovvia restrizione di limitare l'osservazione ad una sola cellula per volta. Il Ca^{2+} imaging di fettine caricate con l'indicatore Ca^{2+} sensibile OGB1-AM ha invece permesso di monitorare allo stesso tempo diversi neuroni a diverse distanze dalla pipetta iniettante KCl dopo lo stesso stimolo. L'esecuzione simultanea di patch clamp e Ca^{2+} imaging nella stessa fettina ha dimostrato una generale correlazione tra le diverse fasi dei cambiamento di voltaggio registrate in current-clamp ed i picchi nelle tracce di fluorescenza. I possibili significati fisiologici e gli eventuali ruoli nell'induzione e nella propagazione della CSD di queste diverse fasi non sono ancora chiari e sono al momento attuale oggetto di studio nel laboratorio dove ho svolto la mia attività di ricerca.

Gli esperimenti di Ca^{2+} imaging hanno permesso, oltre a quanto già descritto, di osservare incrementi nella concentrazione intracellulare di Ca^{2+} degli astrociti in risposta agli stimoli di KCl. Gli astrociti possono sostenere ed amplificare la trasmissione eccitatoria glutamatergica tramite rilascio di glutammato che agisce specificamente sui recettori NMDA; il rilascio di glutammato e di altre sostanze da parte degli astrociti è indotto da innalzamenti nella $[Ca^{2+}]_{int}$, causati a loro volta dal rilascio di diversi neurotrasmettitori (tra cui il glutammato) da parte dei neuroni. Per verificare se la comunicazione reciproca tra neuroni ed astrociti possa essere coinvolta nell'induzione e nella propagazione della CSD, la soglia e la velocità della CSD sono state misurate prima e dopo l'inibizione degli aumenti di Ca^{2+} intracellulare tramite applicazione di acido ciclopiazonico (CPA, 50 μM), in grado di svuotare gli stores di Ca^{2+} intracellulari senza influenzare la risposta dei neuroni al KCl. L'applicazione di CPA non influenzava né la soglia di induzione della CSD, né la velocità di propagazione sia nei topi WT che nei topi KI. Questi risultati suggeriscono che l'intercomunicazione tra neuroni ed astrociti non sia rilevante per l'induzione e la propagazione della CSD.

La combinazione di Ca^{2+} imaging e patch clamp ha permesso l'osservazione, in assenza di stimolazione esterna, di attività spontanea che avviene normalmente nei networks neurali della neocorteccia; tale attività si presenta come oscillazioni lente tra periodi di depolarizzazioni indotte da attività sinaptica associate all'insorgenza di potenziali d'azione (*up-states*) e tra altri periodi in cui l'attività sinaptica diminuisce ed il *firing* scompare (*down-states*). Allo stesso tempo è stato possibile osservare la

presenza di intense oscillazioni spontanee nella $[Ca^{2+}]_{int}$ degli astrociti. Per verificare se la comunicazione reciproca tra neuroni ed astrociti potesse essere coinvolta nella generazione o nella modulazione dell'attività spontanea neuronale di network, tali oscillazioni spontanee degli astrociti sono state soppresse tramite l'applicazione di CPA. In presenza di CPA gli *up-states* neuronali erano ancora presenti sia nei topi WT, che nei KI, tuttavia nel primo caso si assisteva ad una riduzione significativa nella frequenza degli up-states (41 ± 3%, p = 0.0001), non riscontrabile nel caso dei topi KI (11 ± 6%, p = 0.12). Questi risultai preliminari sono in accordo con un possibile ruolo dell'intercomunicazione tra neuroni ed astrociti nell'attività spontanea dei network neuronali.

Summary

Migraine is a common and highly disabling neurological disorder that affect more than 10% of the general population; in 30% of the migraneours migraine headache is preceded by transient neurological symptoms referred as “migraine aura”. Familial Hemiplegic Migraine type 1 (FHM1) is a rare and very severe autosomal dominant subtype of migraine with aura (MA), that is considered a good model for studying migraine: FHM1 typical attacks resemble general MA attacks, but aura symptoms include also motor weakness or paralysis, often but not always unilateral. FHM1 is caused by mutations in the CACNA1A gene, with encodes the α_1, pore-forming subunit of neuronal $Ca_V2.1$ voltage-gated Ca^{2+} channels, also referred as P/Q-type Ca^{2+} channels.

FHM1 mutations produce gain-of-function of human recombinant $Ca_V2.1$ channels, mainly due to a shift of channel activation to more negative voltages and an increase of the open probability and single channel influx over a wide voltage range (Hans et al., 1999; Tottene et al., 2002, 2005; Pietrobon).

Facilitation of experimentally induced cortical spreading depression (CSD) in knock-in (KI) mice carrying the human FHM1 mutation R192Q has been observed in vivo (van den Maagdenberg et al., 2004) and in vitro (Tottene et al., 2009). CSD, a wave of strong neuronal and glial depolarization that slowly progresses across the cerebral cortex, followed by long-lasting neural suppression, is the phenomenon underlying migraine aura and a likely primary cause of migraine headache.

Tottene et al. (2009) recently demonstrated enhanced excitatory neurotransmission due to increased action potential-evoked Ca^{2+} influx through $Ca_V2.1$ channels and increased probability of glutamate release at cortical pyramidal cell synapses of R192Q KI mice. Using an in vitro model of CSD Tottene et al. also demonstrated a causative link between enhanced glutamate release and facilitation of CSD induced by brief pulses of high KCl in cortical slices of KI mice. These findings support a key role of $Ca_V2.1$ channels in CSD initiation and propagation.

In the first part of my Ph. D project I further investigated the mechanisms of CSD induction and propagation and in particular the role of NMDA receptors and voltage-gated calcium channels. Results obtained were published in Tottene el al., 2011 (pdf attached in chapter 3). We adopted the in vitro model of CSD described in Tottene et al., 2009 and measured CSD threshold and velocity in acute cortical slices from WT mice before and after application of specific blockers. CSD was induced by pressure pulses of high KCl of increasing duration; the duration of the first pulse eliciting a CSD was taken as CSD threshold and the rate of horizontal spread of the change in intrinsic optical signal produced by CSD as CSD velocity. We investigated the role of NMDA

using the general NMDA receptors inhibitor D-AP5 (50 μM). In the presence of D-AP5 stimuli up to 30-time the duration of the control threshold failed to induce a CSD. We investigated also the role of P/Q, N, R, and L-type voltage-gated calcium channels using the respective specific blockers: ω-agatoxin IVA (300 nM), ω-conotoxin GVIA (1 μM), SNX-482 (250 nM), and nimodipine (50 μM). Similarly to what observed after application of D-AP5, in the presence of ω-AgaIVA stimuli up to 30-time the duration of the control threshold failed to induce a CSD. Application of either ω-CgTxGVIA and SNX-482 only slightly increased CSD threshold (of about 10%) and slightly decreased CSD velocity (of about 15%) suggesting that N- and R-type voltage-gated Ca^{2+} channels may have a modulatory role in CSD induction and propagation. Application of nimodipine did not affect CSD induction nor propagation. The findings that application of D-AP5 or ω-AgaIVA inhibits CSD induction while ω-CgTxGVIA, SNX-482 and nimodipine have only a poor or null effect are consistent with and support a model of CSD initiation and propagation in which activation of presynaptic (and possibly postsynaptic) $Ca_V2.1$ channels and NMDA receptors plays a pivotal role (Tottene et al., 2011).

The role of NMDA receptors was further investigated in FHM1 R192Q mice, which show an increased glutamate release from pyramidal neurons. In contrast to what happens in WT mice, application of D-AP5 in brain slices from KI mice did not prevent CSD induction, but significantly increased CSD threshold (90 ± 9%) and significantly decreased CSD velocity (47 ± 1%) relative to control. The different effect of D-AP5 in WT and KI mice suggests that other elements (beside NMDA receptors) could be involved in CSD initiation mechanisms.

Current clamp recordings close to the KCl injection pipette (at fixed distance of 100 and 200 μm) allowed to observe different phases in voltage changes after the application of both sub-threshold and threshold KCl stimuli: it was possible, in fact, to distinguish three distinct peaks. While the first two peaks were present in both sub-threshold depolarizations and CSD, the third peak was specifically linked to CSD. Patch-clamp technique allowed to accurately describe different CSD phases but showed the obvious limitation to be restricted to only one cell. Ca^{2+} imaging of slices loaded with the Ca^{2+} sensitive indicator OGB1-AM allowed to observe several neurons at different distances from KCl-injecting pipette at the same time for each pulse. Simultaneous patch-clamp recordings and Ca^{2+} imaging showed a general correlation between voltage changes recorded in current-clamp and fluorescence peaks detected in Ca^{2+} traces. The physiological meaning of these different phases and their specific role in CSD induction and propagation are not clear and are currently object of study in our laboratory.

Ca^{2+} imaging allowed to detect also intracellular calcium increases from astrocytes in response to KCl pulses. Astrocytes can support and amplify glutamatergic synaptic transmission by releasing glutamate that specifically act on NMDA receptors; astrocytic release of glutamate and other substances is induced by $[Ca^{2+}]_{int}$ increases that are, in turn, stimulated by neuronal release of glutamate and other neurotransmitters. To test whether the neuron-astrocyte crosstalk is involved in CSD induction and propagation, threshold for CSD induction and velocity of CSD propagation were measured before and after inhibiting astrocytic $[Ca^{2+}]_{int}$ increases by the application of cyclopiazonic acid (CPA, 50 μM), that emptied astrocytic Ca^{2+} internal stores without affecting neuronal response to KCl. CPA application did not affect CSD threshold or velocity in both WT and KI mice. These results show that neuron-astrocyte crosstalk seem not to be relevant in CSD induction and propagation.

The combination of Ca^{2+} imaging and patch clamp recording permitted to observe, in the absence of external stimuli, spontaneous activity that occurs in the neocortical neural networks as slow oscillations between periods of synaptically-driven depolarizations with firing (up-states) followed by decreased synaptic inputs and ceasing of firing (down-states). At the same time spontaneous large Ca^{2+} oscillations were observed in astrocytes. To check whether neuron-astrocyte crosstalk could be involved in the generation or in the modulation of spontaneous neuronal network activity, astrocytic spontaneous oscillations were inhibited by application of CPA. In presence of CPA up-states were still present in both WT and KI mice; however CPA application led to a significant reduction of up-states frequency in WT (41 ± 3%, $p = 0.0001$), but not in KI mice (11 ± 6%, $p = 0.12$). These preliminary results are in agreement with a possible role of neuron-astrocyte crosstalk in spontaneous neuronal network activity.

1. INTRODUCTION

1.1 Voltage-gated Ca^{2+} channels

Ca^{2+} ions are fundamental for the physiology of all organisms, being involved in a broad spectrum of physiological processes at both cellular and systemic level. The Ca^{2+} ions represent intracellular second messengers in both neurons and non-excitable cells.. Even small changes in the intracellular concentration of Ca^{2+} mediate important processes in cell function.

In excitable cells, [Ca^{2+}] variations are mainly mediated by Ca^{2+} influx through voltage-gated Ca^{2+} channels and thus transduce electrical signals into chemical signals. In skeletal, cardiac and smooth muscle cells cytosolic [Ca^{2+}] variations due to voltage-gated Ca^{2+} channels initiate contraction directly or indirectly, by activation of Ca^{2+}-dependent Ca^{2+} release from sarcoplasmic reticulum. In endocrine cells [Ca^{2+}] influx through voltage-gated channels mediates hormone secretion. In neurons, Ca^{2+} influx through voltage-gated channels triggers neurotransmitter release, mediates dendritic Ca^{2+} transients and regulates different biochemical processes such as enzyme activity and gene expression (Catterall, 2011).

1.1.1 Molecular properties and structure of voltage-gated Ca^{2+} channels

Voltage-gated Ca^{2+} channels belong to a wide superfamily of transmembrane ion channels protein that comprises also voltage-gated potassium and sodium channels (Yu and Catterall, 2005). Voltage-gated Ca^{2+} channels are multiunit complexes formed by a principal transmembrane α_1 subunit associated with other auxiliary subunits: $\alpha_2\delta$, β and eventually γ subunits.

The α_1 is a large 190-250 kDa transmembrane subunit that comprehends the channel pore, the voltage sensors segments and most of the regulatory sites. The amino acid sequence of α_1 subunit is about 2000 residues in length and is organized in four repeated domains (I-IV), each one contains six transmembrane α-helix segments (S1-S6) and a membrane-associated P-loop between S5 and S6 segments. The S4 segments, from the four homologous domains, constitute the voltage-sensor, whereas the S5 and S6 segments and the P-loops between them form the channel pore; each S5-S6 loop contains a pair of glutamate residues that are required for the Ca^{2+} selectivity (Heinemann et al., 1992).

α_1 subunit is in association with a disulfide-linked $\alpha_2\delta$ dimer of 170 kDa, an intracellular phosphorylated β subunit of 50-65 kDa and in some cases with a 33 kDa γ subunit. The extracellular extrinsic membrane α_2 glycoprotein is linked by a disulfide

bond to the transmembrane δ one. The α_2 and δ subunits are encoded by the same gene and the mature forms of these proteins are produced by the post-traslational proteolytic cleavage of the prepolypeptide (De Jongh et al., 1990). Different genes encoding four $\alpha_2\delta$ isoforms ($\alpha_2\delta$-1, -2, -3, -4) have been revealed (Arikkath and Campbell, 2003; Klugbauer et al., 1999); these isoforms have selective effects on the expression level and on the voltage-dependence of different α_1 subunits (Davies et al., 2007). Four different genes codifying different β subunit isoforms have been identified (β-1, -2, -3, -4) and each one can undergo alternative splicing, yielding to a greater isoforms final number; association with different β subunits alters the biophysical properties (e.g. kinetics, voltage dependence of gating) of α_1 subunit. The γ subunit is a transmembrane glycoprotein with four domains that is a component of muscle-specific voltage-gated Ca^{2+} channels; however a related series of seven γ-subunit-like proteins expressed in brain and other tissues have been found: these proteins can modulate the voltage-dependence of $Ca_V2.1$ channels expressed in nonneuronal cells, but it remains to be clarified whether they are associated with voltage-gated Ca^{2+} channels in vivo (Catterall, 2011).

In spite of the high variety of auxiliary subunits that can differently modulate the property of the channel, the different electrophysiological and pharmacological properties of voltage-gated Ca^{2+} channels are mainly due to different α_1 subunits (Hoffmann et al, 1994).

1.1.2 Classification of voltage-gated Ca^{2+} channels

It is possible to classify voltage-gated Ca^{2+} channels on the basis of the Ca^{2+} currents recorded in different cel types. These currents are distinguished in different classes on the basis of their different electrophysiological and pharmacological properties and are categorized by an alphabetical nomenclature. Ten different types of current have been distinguished and characterized by cDNA cloning and functional expression in mammalian cells or *Xenopus leavis* oocytes. These ten types of channels are divided in two major groups on the basis of the voltage depolarization necessary to activated them: low voltage activated (LVA) and high voltage activated (HVA) (Hille et al, 2001). The first group of channels present activation by small depolarization and very fast activation and inactivation kinetics, leading to transient currents; for this reason these channels are referred as T-type Ca^{2+} channels.

Contrarily to the LVA, HVA Ca^{2+} channels are activated by strong depolarization and exhibit slower kinetics. Due to the different activation and inactivation kinetics of HVA Ca^{2+} channels are typically classified on the base of their pharmacological properties. L-type Ca^{2+} channels are inhibited by dihydropyridines (DHPs), phenylalkylamines and

benzothiazepines. Other types of HVA Ca^{2+} channels are not sensitive to L-type Ca^{2+} channels blockers, but are blocked by toxins. N-type Ca^{2+} channels are specifically and irreversibly blocked by ω-conotoxin GVIA (ω-CgTxGVIA), from the venom of the *Conus geographus* snail; P/Q-type Ca^{2+} channels are specifically and irreversibly blocked by ω-agatoxin VIA (ω-AgaVIA) from the venom of the *Agelenopis aperta* spider and by ω-conotoxin MVIIC (ω-CgTxMVIIC) from the venom of the *Conus magus* snail, that however reversibly blocks also N-type Ca^{2+} channels. R-type Ca^{2+} channels are resistant to antagonists, but some R-type Ca^{2+} channels isoforms are specifically blocked by the SNX-482 peptide from the venom of the *Hysterocrates gigas* spider.

T-type Ca^{2+} channels are not sensitive to the organic blockers and the toxins used to block HVA Ca^{2+} channels and there are no widely useful pharmacological tool to block them (Perez-Reyes, 2003).

Mammalian α_1 subunit of voltage-gated Ca^{2+} channels are encoded by at least ten genes (CACNA1S, C, D, F, A, B, E, G, H, I) and, as reported above, ten different types of Ca^{2+} current can be distinguished. Apart from the pharmacologically based partition these ten types of C2+ channels can be divided into three structurally and functionally related families: Ca_V1, Ca_V2 and Ca_V3 (Snutch and Reiner, 1992; Ertel et al, 2000). The alphabetical nomenclature for Ca^{2+} channels is based on the well established K^+ channel nomenclature: Ca^{2+} channels are named using the chemical symbol of the principal permeating ion (Ca) with the principal physiological regulator (voltage) indicated as a subscript (Ca_V); the numerical identifier corresponds to the Ca_V channel α_1 subunit gene subfamily (1 to 3) and the order of discovery of the α_1 subunit within that subfamily (1 through n). Ca_V1 type of α_1 subunit ($Ca_V1.1$ through $Ca_V1.4$) comprises channels containing α_1 S, α_1 C, α_1 D, and α_1 F, subunits; these channels mediate L-type Ca^{2+} currents. Ca_V1 family have about 75% of amino acid sequence identity among them. Ca_V2 family of α_1 subunit share <40% amino acid sequence with Ca_V1 family, but Ca^{2+} channels belonging to Ca_V2 family have >70% amino acid sequence identity among them. $Ca_V2.1$ subfamily includes channels containing the subunit α_1 A, that conduct P/ Q-type Ca^{2+} currents (Mori et al., 1991; Starr et al., 1991); $Ca_V2.2$ and $Ca_V2.3$ channels contain respectively α_1 B and α_1 E subunities and conduct respectively N- (Dubel et al., 1992; Williams et al., 1992) and R-type currents (Soong et al., 1993). Ca_V3 family of Ca^{2+} channels ($Ca_V3.1$ through $Ca_V3.3$) includes channels containing α_1 G, α_1 H, and α_1 I subunities which mediate T-type Ca^{2+} currents (Perez-Reyes et al., 1998). This family is poorly related with others, with an amino acid sequence identity of only 25%. The dichotomy between LVA (Ca_V3) and HVA (Ca_V1 and Ca_V2) Ca^{2+} channels can reflect a very early divergence between two lineages during evolution of multicellular organisms, since single homologues of genes belonging to Ca_V1, Ca_V2 and Ca_V3

subfamilies are found also in invertebrate genomes, including the model organisms *Caenorhabditis elegans* and *Drosophila. sp*.

1.1.3 Localization and function of voltage-gated Ca^{2+} channels

Different subunit are expressed in different locations where they perform different physiological functions (Catterall et al., 2005). With the exception of $Ca_V1.1$, all voltage-gated Ca^{2+} channels are expressed in the brain, with differential distribution in different neuronal populations and different neuronal localization.

Ca_V1 channels couple excitation with different cellular responses, depending on different tissue localization (reviewed in Catterall et al., 2005 and Catteral, 2011). In particular, $Ca_V1.1$ channels are expressed in the skeletal muscle, where they couple excitation with contraction; $Ca_V1.2$ channels are localized in smooth muscles, heart, endocrine cells, and in the soma and proximal dendrites in neurons; $Ca_V1.3$ are distributed in endocrine cells, in neuronal soma and dendrites, and in the cochlea. $Ca_V1.2$ and $Ca_V1.3$ mediate a wide range of functions, from muscular contraction and cardiac pacemaker activity to hormone release in endocrine cells, hearing in cochlea, and neuronal excitability and gene expression in the brain. $Ca_V1.4$ are exclusively expressed in retina, where they mediate neurotransmitter release.

$Ca_V2.1$ and $Ca_V2.2$ in neurons are expressed at the presynaptic terminals, where they initiate neurotransmission, and in the somatodendritic membranes. P/Q-type and N-type Ca^{2+} current mediated by $Ca_V2.1$ and $Ca_V2.2$, respectively, are the predominant pathway for Ca^{2+} entry initiating fast release of classical neurotransmitters, including glutamate, acetylcholine or GABA (Catterall et al., 2005). $Ca_V2.3$ channels are mainly expressed in cell bodies and dendrites where they mediate neuronal excitability (Catterall et al., 2005), but are also localized in presynaptic terminals of some central synapses where they contribute to neurotransmitter release (Gasparini et al., 2001). Ca_V2 channels are expressed also in different endocrine cells and heart (Catterall et al., 2005). Local Ca^{2+} entry through Ca_V2 channels, that are in close proximity to the Ca^{2+} sensors, initiates fast synchronous neurotransmitter release by triggering the fusion of readily releasable neurotransmitter vesicles with the presynaptic membrane, through interaction with several protein at the active zone, including the SNARE complex (Catterall and Few, 2008). Presynaptic $Ca_V2.1$ and $Ca_V2.2$ interacts directly with SNARE proteins through a specific synaptic protein interaction site and this interaction is Ca^{2+} dependent (Catterall., 2011). $Ca_V2.1$ channels play an important role in initiating action potential (AP)-evoked neurotransmitter release at central nervous system synapses (Pietrobon, 2005). At many central synapses P/Q-, N- and R-type Ca^{2+} channels cooperate in controlling neurotransmitter release, but P/Q-type Ca^{2+} channels play a major role,

partly because of a more efficient coupling to the exocytotic machinery (Mintz et al, 1995; Li et al, 2007; Qian and Noebels, 2001; Wu et al, 1999). The preferential localization of P/Q-type Ca^{2+} channels close to the vesicles at the release sites may account for the greater coupling effectiveness of P/Q-type Ca^{2+} channel to release at the Calyx of Held and maybe at other central synapses (Wu et al., 1999).

$Ca_V3.1$ and $Ca_V3.2$ channels are expressed in a wide range of cell types: endocrine cells, smooth muscle, heart, ovary, and placenta. In the cardiac sino-atrial node they largely contribute to the pacemaker current generating heartbeat (Mangoni et al., 2006). In the adrenal cortex they contribute to aldosterone synthesis and secretion (Welsby et al., 2003). In neurons Ca_V3 channels are localized in neuronal soma and dendrites where they are involved in shaping the action potential, in controlling thalamic rhythmic bursts of repetitive firing (i.e thalamic oscillations), and in neuronal integration (Catterall et al., 2005).

1.2 Glutamate receptors

Glutamate is the main excitatory neurotransmitter in the brain: Ca^{2+} dependent glutamate release from excitatory neurons activates various postsynaptic glutamate receptors that can elicit different physiological responses. Glutamate receptors are mainly divided into ionotropic (ligand-gated) and metabotropic (G-protein-coupled) receptors .

Ionotropic glutamate receptors play central roles in a variety of physiological processes, such as basic information processing and changes in synaptic efficacy (e.g learning, memory, development of cellular connections, pain perception) (Bliss and Collingridge, 1993; Woolf and Salter, 2000). A detailed description of ionotropic glutamate receptors is provided in paragraph 1.2.1.

Eight types of metabotropic glutamate receptors have been characterized (mGlu1 through mGlu8); these receptors are divided in three groups (I through III) according to their sequence homology, transduction mechanisms and pharmacology. Group I includes mGlu1 and mGlu5, that are localized predominantly postsynaptically, with a location adjacent to the margins of the synaptic cleft; mGlu1, but not mGlu5 is present also in glia. Group II receptors include mGlu2 and mGlu3, that are mainly presynaptic and are predominantly located on the axon; mGlu3 is present also in glia. Group III includes mGlu4, mGlu6, mGlu7 and mGlu8, that are also presynaptic (Moldrich et al., 2003). Group I receptors are coupled to a Gq protein and activate phospholipase C (PLC) and the subsequent Ca^{2+}-phosphoinositides biochemical pathway; the activation of these pathways lead to activation of voltage-gated Ca^{2+} channels and induction of K^+ efflux via Ca^{2+}-sensitive K^+ channels. Groups II and III receptors are coupled to a Gi

protein , that inhibits adenylate cyclase activity and decrease the formation of cyclic adenosine monophosphate (cAMP), which can result in the inhibition of voltage-gated Ca^{2+} channels. Metabotropic glutamate receptors have a wide range of effects on neurons and glia (reviewed in Cartmell and Schoepp, 2000; Schoepp, 2001) and exhibit activity-dependent plasticity.

1.2.1 Ionotropic glutamate receptors

Ionotropic glutamate receptors show many differences in their biophysical, pharmacological and modulatory properties. In spite of this glutamate receptor ion channels share a similar structure and share also evolutionary proximity and structural similarity with K^+ channels family (Wollmuth and Sobolevsky, 2004). Ionotropic glutamate receptors are transmembrane proteins composed by four large subunits, each one of them is a modular structure that contains four domains: an extracellular amino-terminal domain (ATD), an extracellular ligand-binding domain (LBD), the transmembrane domain (TMD), and an intracellular carboxyl-terminal domain (CTD). The ATD and LBD assemble ad dimers of dimers; two conformationally distinct organizations of the dimers forms two conformationally different subunits, which are denoted A/C and B/D subunits; A/C and B/D subunits will couple differently to the ion channel domain, with different effects on the glutamate receptor functionality (Traynelis et al., 2010). The LBD is highly conserved within the whole family of glutamate receptors: it is composed by two extracellular segments called S1 and S2 (Stern-Bach et al., 1994). LBD is structurally shaped in a clamshell-like configuration, with the two segment S1 and S2 forming most of the two halves of the clamshell (D1 and D2): the ligand binding site is locate in the middle of structure, between D1 and D2. In the ligand-unbound or antagonist-bound configurations D1 and D2 are separated and form an open cleft structure; in the ligand-bound conformation D1 and D2 form a closed cleft structure. This ligand-induced (or agonist-induced) closed configuration is an early conformational event that triggers the conformational transition of the ion channel domain to the open state. The extracellular ATD domain does not play an essential function for the core functions of ionotropic glutamate receptors, but plays only regulative functions; ATD contains binding sites for divalent cations, such as Zn^{2+}, subunit-selective negative allosteric modulators, and may contain binding sites for extracellular proteins (Traynelis et al., 2010). TMD is characterized by four hydrophobic transmembrane domains (M1 through M4); three transmembrane helices, M1, M3, and M4 from the four subunities contribute to form the ion channel pore. M2 loops line the inner pore cavity, whereas M3 helices line the outer one and presumably form the gate occluding the pore in the closed-state channel configuration. CTD is the

most variable domain between the different types of ionotropic glutamate receptors and shows no sequence homology to any known protein. This domain is thought to regulate membrane targeting, stabilization, post-translational modifications and targeting for degradation.

A residue located an the apex on the M2 loop, referred as QRN site, plays a critical role in determining the single-channels permeability, conductance, and pharmacological properties of the glutamate receptor ion channel. These receptors are all cation-permeable, but not all are permeable to Ca^{2+}; glutamate receptors show a wide range of single-channel conductance (Traynelis et al., 2010). Glutamate receptors function can be regulated by endogenous ions, including Zn^{2+}, Mg^{2+}, and polyamines, that have voltage-dependant block mechanisms.

Ionotropic glutamate receptors are divided in four classes on the base of their different structural homology and pharmacological properties: α-amino-3-hydroxy-5-methyl-4-isoxazolepropionic acid receptors (AMPA receptors), that comprehend GluA1 through GluA4 subunits; kainate receptors, that include GluK1 through Gluk5 subunits; N-methyl-D-aspartate receptors (NMDA receptors), that comprehends GluN1, GluN2A through GluN2D, GluN3A, and GluN3B subunits, and the δ receptors, that include GluD1 and GluD2 subunits.

AMPA receptors show rapid activation and deactivation kinetics, rapid and strong strong desensitization, that lead to short transient currents. These receptors are poorly Ca^{2+}-permeable and are blocked by intracellular polyamines (Treynelis et al., 2010). Within mammalian brain AMPA receptors mediate the majority of fast excitatory synaptic transmission.

Kainate receptors, like AMPA ones, show relatively fast gating kinetics and strong desensitization, but kainate synaptic currents are slower than AMPA ones (Castillo et al., 1997; Kidd and Isaac, 2001). Unlike AMPA and NMDA receptors, kainate receptors can play important roles both pre- and postsynaptically. In addition to the ionotropic role, kainate receptors can also signal by G protein, acting as metabotropic receptors (Rodríguez-Moreno and Lerma, 1998).

1.2.2 NMDA glutamate receptors

N-methyl-D-aspartate receptors (NMDA receptors) are critically involved in excitatory synaptic transmission, synaptic plasticity and excitotoxicity in the brain. Their unique features include the requirement for activation of the co-agonist D-serine (or glycine), voltage-sensitive block by extracellular Mg^{2+}, high permeability to Ca^{2+}, and slow gating kinetics, with relatively weak or no desensitization. Together these

features confer to NMDA receptors the unique role of “coincidence detector”, able to finely integrate synaptic activity.

NMDA receptors include three families of subunits: GluN1, GluN2, and the recently identified GluN3 (Moriyoshi et al., 1991; Monyer et al., 1992; Mori and Mishina, 1995); these subunits correspond to NR1, NR2, and NR3 subunits according an old nomenclature (Collingridge et al., 2009). NMDA receptors assembly as heterotetramers, usually associating two obligatory GluN1 and two GluN2 subunits; NMDA receptors which include GluN3 subunits are though to form either diheteromeric complexes (GluN1/GluN3) or triheteromeric complexes (GluN1/GluN2/GluN3) (Traynelis et al., 2010). GluN1 subunits are encoded by a single gene but are found as eight different isoforms (GluN1-1a through GluN1-4a and GluN1-1b through GluN1-4b) arising from alternative RNA splicing (Dingledine et al., 1999); “b” isoforms are longer than “a” ones, containing an additional 21 amino acid stretch, called N1 cassette, which significantly affects functionality of the receptor. GluN1 subunits are ubiquitously expressed in CNS: GluN1-1 is expressed mostly in rostral structures and GluN1-4 has principally a caudal expression; GluN1-3 subunits are expressed only at very low levels.; expression pattern of “a” and “b” variants are overlapping, but “a” forms are more abundant in most, but not all, brain regions. GluN2 subunit family comprehends four members (GluN2A through GluN2D), that are encoded by four different genes. GluN2 subunits present both developmental and spatial expression patterns (Paoletti, 2011). Initially in rodent embryos only GluN2B and GluN2D are expressed, but the expression pattern changes rapidly during the first two weeks after birth. In the adult GluN2A is highly expressed in the whole brain, while GluN2b is restrictedly expressed in the forebrain areas (cortex, hippocampus, striatum, olfactory bulb), GluN2C is present in cerebellar granule cells and in the olfactory bulb, and GluN2D is weakly expressed in diencephalon and brainstem. GluN3 family comprehends two members (GluN3A and GluN3B) encoded by two different genes; GluN3A expression is low before birth and in the adulthood and peaks in the early postnatal life, while GluN3B expression is initially low and increases progressively, reaching the maximum in the adulthood. GluN3B was initially though to be expressed only brain stem and spinal chord, but in fact seems to be ubiquitous in the CNS and to be parallel to GluN1 subunits (Wee et al., 2008). Different subtypes assembly can give raise to different subtypes of NMDA receptors.

Subcellular NMDA receptors localization is not only at postsynaptic sites, but also perisynaptic, extrasynaptic, and even at presynaptic sites, where they can influence neurotransmitter release (reviewed in Paoletti, 2011). Subunit composition can vary according to the subcellular localization: for example GluN2B subunits are abundant at

extrasynaptic sites and GluN2D are almost exclusively extrasynaptic, but can be found also at synapses (Cull-Candy and Leskiewicz, 2004; Kohr, 2006; Paoletti, 2011).

NMDA receptor structure fully resemble the general structure of ionotropic glutamate receptor described above.

NMDA receptor activation (i.e. ligand binding and channel gate opening) resemble the general activation mechanism of ionotropic glutamate receptors. These mechanisms can be summarized in a sequence: (i) ligands binding to the central cleft of the clamshell-like structure formed by LBDs, each LBD carrying a single ligand site (GluN1 or GluN3 bind the co-agonist D-serine or glycine and GluN2 binds glutamate); (ii) ligand-binding induces closure of the LBDs cleft and a conformational change that increase separation between LBDs bottom lobes; (iii) this separation in turn induces a further conformational change leading to the reorientation of the TMD transmembrane helices and channel gate open.

NMDA receptors show a strong voltage-dependent Mg^{2+}. The major blocking site for Mg^{2+} is locate at or near the narrow channel constriction; additional voltage-dependence is due to other ions-binding sites in the internal and external channels cavities (Dingledine et al., 1999; Traynelis et al., 2010).

As reported above, different subunits assembly leads to different NMDA receptors subtypes, whit different functional properties. Each aspect of the gating (i.e. sensitivity to agonists, activation/deactivation kinetics, sensitivity to Mg^{2+} ions and kinetics of Mg^{2+}-induced block and unblock, channel mean open time, and channel open probability) is strictly dependant from subunit composition. For example GluN1/GluN2A and GluN1/GluN2B receptors display larger currents and higher Mg^{2+} sensitivity block than GluN1/GluN2C and GluN1/GluN2D ones. Moreover GluN1/GluN2A receptors show relatively low D-serine (or glycine) affinity and the fastest decay (40 ms), while GluN1/GluN2D are the slowest (2s). Also the maximal open probability (P_o) vary a lot, being relatively high (~0.5) for GluN1/GluN2A, intermediate (~0.1) for GluN1/GluN2B, and very low (~0.01) for GluN1/GluN2C and GluN1/GluN2D (reviewed in Traynelis et al., 2010 and Paoletti, 2011). In conclusion, it is possible to distinguish NMDA receptors with long but prolonged activity and other with relatively high, but (relatively) transient activity.

Because of the strong voltage-dependence, due to Mg^{2+} block, NMDA receptors act as coincidence receptors and sense postsynaptic depolarization at the same time (or shortly after) of glutamate, or other excitatory neurotransmitter, presynaptic release. In fact NMDA and AMPA receptors colocalize at all central synapses, thus glutamate released presynaptically activate both type of receptors. This role is well known to be important in contribution to synaptic transmission and associative learning.

1.3 Biology and pathophysiology of migraine

Migraine is an episodic, highly disabling, brain disorder that affects more than 10% of the general population. Typical migraine attacks are characterized by unilateral, intense pulsating headache, lasting 4-72 hours, often accompanied by nausea, photophobia and phonophobia. In about 30% of patients, migraine headache is preceded by transient neurological symptoms, called “migraine aura” (MA); these symptoms are mostly visual, but they can also involve other senses or, rarely, can cause motor impairments. Migraine visual aura generally consists in a scotoma (an area of lost vision) with a scintillating border, that usually begins near the center of vision as a twinkling star and then develops into an expanding circle that slowly move across the visual field towards the periphery. Migraine has a strong (up to 50%) genetic component, higher in migraine with aura.

Migraine headache arises with the activation of the trigeminovascular system (Dalkara et al., 2006); indeed, within the skull, pain sensitivity is primarily restricted to the meningeal blood vessels, which are densely innervated by nociceptive sensory afferent fibers of the ophthalmic division of the trigeminal nerve (Pietrobon, 2005; Pietrobon and Striessnig, 2003). In several animal model, including non-human primates, it has been observed that trigeminovascular meningeal afferents stimulation leads to activation of second order neurons of dorsal horn neurons in the trigeminovascular nucleous parts caudalis (TNC) and the two uppermost divisions of the spinal cord. Signalling then proceed rostrally to central regions deputed to pain perception, including several thalamic nuclei and the ventrolateral area of the caudal periaqueductal grey regions (PAG). PAG contributes to pain generation not only through ascending projections to the thalamus, but also through descending modulation (mainly inhibitory) of nociceptive afferent information via projections to serotonergic neurons in the magnus raphae nucleus (MRN) (Knight and Goadsby, 2001). Activation of the trigeminovascular system leads also to the the peripheral release of different vasoactive neuropeptides, including substance P (SP), neurokinin A (NKA), and especially the calcitonin gene-related peptide (CGRP). Other vasoactive neuropeptides as vasoactive intestinal peptide (VIP), nitric oxide (NO), and acetylcholine (ACh) are released in the meninges by parasympathetic efferents from the superior sphenopalatine ganglion (SPG), that are activated by stimulation of the superior salivatory nucleus (SSN) through the trigeminal ascending projections. Vasoactive neuropeptides induce a phlogosis process (neurogenic inflammation), that in animal studies has been shown to comprehend vasodilation of meningeal vessels, mainly due to CGRP, plasma extravasation and mast cells degranulation, with consequent further release of other proinflammatory substances in the dura mater. Evidence of activation of the

trigeminovascular system in humans during migraine is provided by increased levels of CGRP (but, interestingly, not of SP) in both external and internal jugular blood during migraine attacks (Goadsby et al., 1990; Sarchielli et al., 2000); these increased levels return back to physiological levels after headache cessation after treatment with the specific anti-migraine drug sumatriptan (Goadsby and Edvinsson, 1993).

One of the first theories aiming to explain migraine mechanisms was the so called "vascular" theory, proposed by Penfield, 1935 and by Ray and Wolff, 1940, who suggested that the symptoms of migraine aura were caused by transient ischemia induced by vasoconstriction, and the headache arose from rebound abnormal vasodilatation of intracranial arteries and consequent mechanical activation of perivascular sensory fibers (Pietrobon and Striessnig, 2003). Once widely accepted, in the last decades this theory has become obsolete, being contradicted by several evidences (Charles, 2009). In fact functional brain imaging during MA attacks shows spreading cortical hyperaemia, followed by oligaemia, which outlasts the aura symptoms, extending into the headache phase (Olesen and Larsen, 1981).

Recent findings point to cortical spreading depression (CSD) as the main mechanism for the pathogenesis of migraine (Pietrobon, 2005; Pietrobon and Striessnig, 2003, Levy et al., 2011).

1.4 Cortical spreading depression (CSD)

After the discovery of migraine visual aura in 1941 by Karl Lashley, Leao (1944) discovered in the rabbit cerebral cortex an electrophysiological correlated that termed cortical spreading depression (CSD). CSD is inducible in animals by a focal stimulation (mechanical, electrical of with high KCl) and is described as a slow wave (2-6 mm/min) of strong neuronal and glial depolarization that progresses across the cerebral cortex, generating transient intense neuronal spike activity, followed by long-lasting neural suppression (Charles and Brennan, 2009; Lauritzen, 1994; Pietrobon, 2005). After the transient, strong depolarization to almost 0 mV, that precludes any action potential generation or synaptic transmission, cerebral function is suppressed for a relatively long time: although resting membrane potential is typically restored within a minute, the complete recovery of synaptic functionality may take 10 minutes or more. The first depolarization phase is coupled with a transient vasodilatation, followed by increasing regional cerebral blood flow (rCBF); subsequently, the phase of impaired neuronal activity associates to a reduction in rCBF, following a sustained vasoconstriction. CSD has been indicated by neuroimaging findings as the responsible for migraine visual aura (Pietrobon and Striessnig, 2003). CSD occurrence has never been observed in humans during electroencephalographic recordings over surgery. In spite of this, blood

oxygenation level-dependent functional magnetic resonance imaging (BOLD fMRI) with near-continuous recording in patients during visual aura showed typical CSD-correlated cerebrovascular changes. A clear temporal correlation has been observed between the initial features of the aura (scintillations beginning in the paracentral left visual field) and the initial increase in the mean BOLD signal, reflecting cortical hyperaemia (Hadjikani et al., 2001). The subsequent decrease in mean BOLD level showed temporal correlation with the scotoma. The BOLD signal changes developed first in the extrastriate cortex, contralateral to the visual changes, and then slowly migrated (3.5 mm/min) towards more anterior regions of the visual cortex, representing peripheral visual fields, in agreement with the progressive movement of the scintillations and scotoma from the center of vision towards the periphery. Spreading cerebral perfusion changes have also been observed in migraine without aura, suggesting the possibility that CSD can occur also in patients presenting migraine without aura. In this case CSD may induce headache without eliciting aura symptoms because it originates in a clinically silent area of the cerebral cortex (Dalkara et al., 2006; Pietrobon, 2005). Moreover, magnetoencephalography has further demonstrated the presence of an electrical activity similar to CSD during visual aura (Bowyer et al., 2001).

Evidences pointing to CSD as the electrical phenomenon underlying migraine aura symptoms are today widely accepted; despite this, the question whether CSD can trigger migraine headache is still controversial and highly debated (Ayata, 2010). This question assumes important clinical implications: if CSD triggers migraine headache, pharmacological CSD targeting may constitute a remarkable new approach for migraine therapy and prophylaxis. Recent findings provided by animal studies support the hypothesis of CSD as migraine headache trigger (Pietrobon, 2005, 2007). First it has been clearly demonstrated that CSD is able to directly activate the meningeal nociceptors (Zhang et al., 2010) and to elicit a long-lasting blood-flow increase within the middle meningeal artery and plasma protein leakage in the dura mater (Bolay et al., 2002). CSD induces strong changes in cortical extracellular medium and in particular it induces large increases in the concentration of K^+ and H^+ ions, the vasoactive substances NO, arachidonic acid, and prostaglandins and the nociceptive messenger ATP. (Pietrobon and Striessnig, 2003) Many of these substances can activate the meningeal trigeminovascular afferents, either directly or by causing perivascular inflammation (Charles and Brennan, 2009; Pietrobon, 2005). Moreover, five migraine prophylactic drugs belonging to different pharmacological classes, (valproate, topiramate, propanolol, amitriptyline, and methysergide) that are effective in reducing the frequency of migraine attacks (with or without aura) have been recently shown to dose-dependently suppress CSD susceptibility in experimental animal models (Ayata et

al., 2006). In spite of these evidences, a direct link between CSD and headache in patients is not already demonstrated. Moreover, in migraineurs CSD is not induced, like in an experimental animal model, but occurs spontaneously in response to specific triggers (e.g. stress, long-lasting repetitive sensory stimulation), with unknown mechanisms. Migraneours are highly sensitive to sensory stimulation and there are strong evidences suggesting altered cortical excitability with abnormal processing of sensory information in their brain in the period between migraine attacks (Aurora and Wilkinson, 2007; Coppola et al., 2007; Pietrobon and Striessnig, 2003). The mechanisms underlying abnormalities in cortical activities in migraine patients and their relationship to CSD occurrence are unclear.

1.5 Familial Hemiplegic Migraine (FHM)

Familial hemiplegic migraine is a rare and very severe autosomal dominant subtype of migraine with aura (MA), that is considered a good model for studying migraine (Pietrobon, 2007). FHM typical attacks resemble general MA attacks, but aura symptoms include also motor weakness or paralysis, often but not always unilateral. Appearance and progression of aura symptoms in FHM and in general MA are similar but in FHM they stay longer; also headache is usually longer in FHM, but other pain characteristic are similar to general MA. FHM and MA attacks often may alternate in FHM patients and can co-occur within FHM families. All these evidences suggest that FHM and MA can some pathogenic mechanism.

Besides “canonical” FHM attacks, some FHM patients sometimes can suffer atypical more severe attack including signs of diffuse encephalopathy, coma, confusion, prolonged hemiplegia (lasting up to several days), and in few cases seizures (Thomsen et al., 2002). In addiction, about 20% of FHM families show permanent cerebellar symptoms of progressive cerebellar ataxia with or without nystagmus (Thomsen et al., 2002).

FHM is a genetically heterogeneous pathology that can arise from mutations in the gene *CACNA1A* at the chromosome 19p13 (Ophoff et al., 1996), *ATP1A2* at 1q23 (De Fusco et al., 2003), and *SCNA1A* at 2q24 (Dichgans et al., 2005); these mutations are responsible for type 1 (FHM1), that represent up to 50% of the cases, type 2 (FHM2), 20-30% of the cases, and type 3 FHM (FHM3), respectively. From the clinical point of view there are few symptomatological differences between genotypes; the only exception is that the onset of permanent cerebellar symptoms is almost exclusively associated with FHM1.

1.5.1 Familial hemiplegic migraine type 1 (FHM1)

As reported above, mutations in the gene *CACNA1A* cause FHM1. *CACNA1A* encodes the α_1 subunit (pore-forming, see paragraph 1.1.1 and 1.1.2) of $Ca_V2.1$ voltage-gated Ca^{2+} channels. Eighteen missense mutations causing FHM1 have been identified; all these mutations have been observed to produce substitution of conserved amino acids in important functional regions, including the pore region and the voltage sensors (Pietrobon, 2007). Moreover pure FHM1 and FHM1 associated with cerebellar symptoms are related to distinct mutations.

$Ca_V2.1$ channels are expressed in all brain portions that are involved in the pathogenesis of migraine in general, including cerebral cortex, trigeminal ganglia, and brainstem nuclei involved in the central nociception control. In particular high levels of $Ca_V2.1$ expression can be found in the cerebellum; deletion of α_1 subunit of these channels, indeed, leads to severe cerebellar ataxia, dystonia and progressive degeneration.

1.5.2 Functional consequences of FHM1

The functional consequences of twelve FHM1 mutations have been examined in heterologous expression systems expressing recombinant $Ca_V2.1$ channels (Pietrobon, 2007). These studies revealed that FHM1 mutations alter in a complex way many biophysical properties of $Ca_V2.1$ channels and in some cases (e.g. inactivation properties) different mutations can lead to different effects. In addiction, five of these twelve mutations have also been investigated in granule cells from $Ca_V2.1$ $\alpha_1^{-/-}$ mice expressing human $Ca_V2.1$ α_1 subunits (Cao et al., 2004, 2005; Tottene et al., 2002, 2005). A consistent common effect of FHM1 mutations has been observed by studying the single channels properties of of eight mutant human $Ca_V2.1$ channels: all these FHM1 mutations showed an increased single channel Ca^{2+} influx in a wide range of mild depolarizations; this reflects an increased open probability of the channels, mainly due to a shift to lower voltages of channel activation (Hans et al., 1999; Tottene et al., 2002; Tottene et al., 2005; Pietrobon, unpublished data).

Recently two knock-in (KI) mouse lines carrying the FHM1 mutations R192Q and S218L were generated by homologous recombination; this allowed the first analysis of FHM1 mutations in endogenously expressed channels (van den Maagdenberg et al, 2004). $Ca_V2.1$ current densities in cerebellar granule cells and cortical pyramidal cells of R192Q and S218L KI mice were larger than wild-type (WT) neurons for a broad range of mild depolarizations. The shift to lower voltages of channels opening

probability and the gain-of-function of the neuronal $Ca_V2.1$ currents were about twice larger in homozygous S218L KI mice compared with heterozygous; this revealed an allele-dosage effect that is consistent with dominance of the mutation in FHM1 patients.

The R192Q (RQ) mutation produces a typical FHM phenotype, with typical attacks. In apparent contrast with this, homozygous RQ mice appear healthy. Changes in whole-cell $Ca_V2.1$ current density in KI neurons were very similar to those found in mutant recombinant human $Ca_V2.1$ channels. Recent findings in cortical neurons microcultures, where excitatory neurotransmission at physiological Ca^{2+} concentration has been studied, demonstrated increased glutamate release due to an increased P/Q-type Ca^{2+} channels contribution (Tottene et al., 2005).

Recently Tottene et al. (2009) demonstrated in both cortical neurons microcultures and brain slices from FHM1 RQ mice gain-of-function of excitatory neurotransmission due to action-potential-evoked Ca^{2+} influx through $Ca_V2.1$ channels and increased probability of glutamate release at pyramidal cells synapses. Contrarily, inhibitory neurotransmission at fast-spiking (FS) interneuron synapses of RQ mice was unaltered.

Interestingly, an increased susceptibility of RQ mice to experimental CSD has been observed, both in vivo (van den Maagdenberg et al., 2004) and in vitro (Tottene et al., 2009) compared to WT. In particular it has been observed a lower threshold for CSD initiation and an increased velocity of propagation of CSD induced by electrical stimulation of the visual cortex in vivo. Similar results have been obtained by Tottene et al. (2009): using an in vitro model of CSD induction by pressure pulses of high KCl in cortical brain slices they demonstrated a causative link between enhanced glutamate release at pyramidal synapses and CSD facilitation in these mice.

1.6 Experimental CSD

As written above CSD can be experimentally induced by focal stimulation, for example with mechanical, electrical, and high KCl stimulation. Stimuli that can produce CSD induce an anomalous increase in the extracellular concentration of K^+ ions, $[K^+]_{out}$, and a sustained neuronal depolarization accompanied by an increase in neuronal firing (Pietrobon, 2007). When stimuli sufficiently intense to ignite a CSD are applied the regulatory mechanisms that normally keep $[K^+]_{out}$ within the physiological range are overwhelmed by the build-up of $[K^+]_{out}$ via a positive feedback cycle that makes self-regenerating the initially gradual neuronal depolarization. This positive feedback cycle initiates when a sufficient number of V-dependent and/or $[K^+]_{out}$-dependent cationic channels are activated to generate a net sustained inward current, with consequent further depolarization and further increase of the local $[K^+]_{out}$, leading to further activation of the cationic channels (Somjen, 2001; Pietrobon, 2007). The nature of these

cationic channels is still unclear and controversial (Somjen, 2001), although there are strong pharmacological evidences supporting a key role of NMDA receptors. The findings of Tottene et al. (2009) are consistent with and support a model of CSD initiation in which activation of presynaptic voltage-gated Ca^{2+} channels (in particular P/Q-type) with consequent release of glutamate from recurrent cortical pyramidal cell synapses and activation of NMDA receptors are key components of the positive feedback cycle that ignites CSD (Pietrobon, 2005b).

Clear evidences have been found supporting the hypothesis that CSD initiates and propagates at the level of the dendrites of pyramidal cells (Somjen, 2001; Pietrobon, 2007) and involves an increased conductance in specific dendritic subregions (Canals et al., 2005). Also CSD propagation mechanisms still remains unclear and very debated. Two main hypothesis have been proposed: interstitial K^+ diffusion initiating in adjacent dendrites the positive feedback cycle that ignites CSD or CSD propagation through gap junctions (Somjen, 2001).

1.7 Spontaneous cortical network activity

During quiescent states in absence of external stimuli, such as natural sleep or anesthesia, the neocortex is no silent, but it exhibits complex electrical activity. In particular, because of the dense local connectivity, the neocortex is engaged in spontaneous high synchronous spontaneous network activity, that can be measured by EEG or extracellular (or intracellular) recording in vivo as slow oscillations. These spontaneous oscillations are characterized by rhythmic <1 Hz cycles of synaptically-mediated sustained depolarizations (about 10 mV in amplitude) and neuronal firing (up-states), followed by decrease of synaptic inputs and cessation of firing (down-states) (Steriade et al., 1993; Haider et al., 2006). Up-states in fact correspond to recurrent synaptic network activity generated within cortical circuitry (Shu et al., 2003): pyramidal-pyramidal connections generate a feedforward network excitation coupled to a simultaneous network feedback and feedforward inhibition due to pyramidal-inhibitory interneurons connections. Network architecture provides a dynamic balance between excitation and inhibition during up-states. This spontaneous network activity originates within the cortex and propagates after to subcortical areas (e.g. thalamus and striate), as deducible from lesion experiments (Amzica and Steriade., 1995). Recent findings point to intrinsically active pacemaker neurons as spontaneous network activity generators: when a sufficient number of these neurons fire simultaneously, postsynaptic neurons are triggered to fire action potentials, recruiting in turn other connected neurons and “turning on” the cortical network (Bazhenov et al., 2002; Le Bon-Jego and Yuste, 2007).

In brain slices, in particular conditions (divalent ions concentrations similar to those found in natural cerebrospinal fluid), it is possible to detect spontaneous network activity similar to that observed in vivo, thus characterized by the presence of cycles of up- and down-states (Sanchez-Vives and McCormick, 2000).

1.8 Astrocytes

Astrocytes belong to the glia cell class that represents the most abundant cells in the brain. Astrocytes are in strict contact with a high number of neurons, blood vessels and other astrocytes. Astrocytes are also coupled by gap-junctions and form the so-called "astrocytic syncytium" (Giaume and McCarthy 1996). Each astrocyte occupies distinct domains with little overlapping with the processes of neighbors astrocytes (Bushong et al. 2002; Halassa et al. 2007b). The first description of astrocytes was made by Rudolph Virchow in 1858 who called these cell neuroglia (nerve glue). For a long time they were considered merely supportive element of brain, unable to participate in information processing, their principal role being structural and metabolic support to neurons. In fact, astrocytes exhibit passive electrophysiological properties and are consequently considered as non-excitable cells. In the last 20 years several studies demonstrated that astrocytes can perform a series of important tasks, including the uptake/recycle of neurotransmitters and the buffering of extracellular potassium and neurotransmitters. Over the last decade, the role of astrocytes in brain information processing has been, however, deeply reconsidered. Initially, several studies demonstrated that cultured astrocytes have the potential to express a large number of transmembrane proteins, including channels and receptors. Studies performed in the early 1990s on acutely obtained brain slices demonstrated that subpopulations of astrocytes and neurons share almost the same set of receptors and channels (for a review, see Seifert et al., 2006). In the same years, glutamate applications were observed to trigger Ca^{2+} elevations and Ca^{2+} waves in hippocampal cultured astrocytes (Parpura et al., 1994). It was also observed that applications of several neurotransmitters, including glutamate, GABA, ATP, and adenosine can induce Ca^{2+} elevations in glial cells from brain slices. Two main hypotheses were made about the transmission mechanisms of Ca^{2+} waves: i) IP3 diffusion through gap junctions, evoking Ca^{2+} signals in neighboring unstimulated astrocytes, and ii) ATP release from an astrocyte which stimulates additional Ca^{2+} changes in adjacent astrocytes through P2Y receptors activation. Although it is likely that both pathways contribute to wave propagation, the evidence that the wave can propagate between physically disconnected cells (Hassinger et al, 1996) suggested a role for an ATP-mediated extracellular signaling. Finally, in 1994 two groups demonstrated that evoked Ca^{2+} increases in cultured astrocytes resulted in activation of

adjacent neurons (Nedergaard, 1994; Parpura et al., 1994). Parpura at al., 1994 suggested that the Ca^{2+}-dependent release of glutamate from astrocytes was the cause of the neuronal depolarization through activation of ionotropic glutamate receptors; other independent studies reproduced these data and provided further evidence for the release of glutamate in the mechanism of neuronal activation (Charles, 1994; Hassinger et al., 1995). These culture studies were confirmed in rat brain slices by Pasti et al. (1997), who demonstrated a bidirectional signaling between astrocytes and neurons and also showed that the activation of astrocytic metabotropic glutamate receptors by synaptically released glutamate evokes glial Ca^{2+} elevations and a delayed Ca^{2+} increased in nearby neurons mediated by ionotropic glutamate receptors. Whole cell recordings from a neuron that was cocultured with astrocytes demonstrated slow glutamate-mediated inward currents (SICs) in coincidence with an astrocytic Ca^{2+} elevation (Araque et al., 1998). These results were later validated in the thalamus and the hippocampus by showing pure NMDA receptor-dependent neuronal currents following astrocytic Ca^{2+} elevations (Fellin et al., 2004; Haydon and Carmignoto, 2006).

Several mechanisms can be at the basis of glutamate release in astrocytes. Experimental evidence has been provided for the existence of at least four distinct pathways for glutamate release in astrocytes: exocytosis, hemichannels, anion transporters, and P2X receptors. The most widely studied is the Ca^{2+}-dependent exocytotic mechanism (Haydon and Carmignoto, 2006). In addition to glutamate, other gliotransmitters can be released through a Ca^{2+} dependent mechanism such as D-serine, ATP, GABA and others.

Cell culture studies initially demonstrated that glutamate released from astrocytes can activate NMDA receptors in nearby neurons (Parpura et al., 1994). This observation was then validated in brain slices in which astrocytic glutamate was shown to selectively act on a specific class of NMDA receptor that contains the GluN2B subunit (Fellin et al., 2004). As written above, GluN1-GluN2B NMDA receptors are mainly expressed extrasynaptically; moreover additional evidences, including double-label immunoelectron microscopy findings (Bezzi et al., 1998), support the hypothesis that the glutamate released from astrocytes selectively acts on extrasynaptic NMDARs that contain the GluN2B subunit. Other forms of synaptic modulation have been identified in which metabotropic glutamate receptors and kainate receptors mediate the actions of glial-released glutamate (Haydon and Carmignoto, 2006). These crucial observations established the presence of an astrocyte-neuron communication system that adds a new level of complexity in the brain network. Indeed, following these initial observations many additional studies demonstrated that gliotransmitters can modulate synaptic transmission and neuronal excitability.

All in all, these studies led to the idea of the “tripartite synapse” in which astrocytes sense synaptic activity and provide a feedback signal that can modulate the strength of the synapse (Araque et al., 1999).

Given the emerging importance of astrocytes in CNS signaling, many studies have been done to clarify whether functional alterations in astrocytes may play a role also in brain disorders.. Evidence for an astrocytic involvement in the etiology of different CNS pathologies have been found in epilepsy, amyothrophic lateral sclerosis (ALS), stroke, focal cerebral ischaemia, and hepatic encephalopathy (Seifert et al., 2006). Recently Gomez-Gonzalo et al. (2010) found that the cooperation between neurons and astrocytes can produce an excitatory loop that contributes to the generation of focal seizures in a new model of focally induced seizure-like discharges in rat entorhinal cortex acute slices.

2. Aim of work (I)

As reported in section 1.6, Tottene et al. (2009) studied cortical neurotransmission in neuronal microcultures and brain slices from FHM1 KI mice. They demonstrated a gain of function in the excitatory neurotransmission due to an increased action-potential-evoked Ca^{2+} influx and increased glutamate release probability at pyramidal cell synapses. They also found unaltered inhibitory neurotransmission at fast-spiking interneuron synapses. Using an in vitro model of experimental CSD focally induced by high KCl pressure pulses, these authors demonstrated a causative link between enhanced glutamate release at pyramidal synapses and CSD facilitation in FHM1 KI mice. These findings were in agreement with a model of CSD initiation and propagation in which the activation of presynaptic P/Q-type Ca^{2+} channels plays a central role.

The first aim of my PhD project was to further investigate the mechanism underlying CSD induction and propagation focusing on the role of both voltage-gated Ca^{2+} channels and NMDA receptors. CSD threshold and velocity (see section 9, Material and methods) were measured in brain slices from WT mice before and after the application of different voltage-gated Ca^{2+} channel blockers and NMDA receptor blocker, such as D-AP5. Since it was unclear whether NMDA receptor–mediated transmission plays only a modulatory role or is required for CSD induction and propagation (Somjen, 2001; Charles and Brennan, 2009), the role of NMDA receptors was further investigated in FHM1 R192Q mice which show an increased glutamate release from pyramidal neurons.

The results obtained in WT mice are reported in Tottene et al. (2011; see the attached pdf in chapter 3). Preliminary results obtained in R192Q KI mice are described in chapter 4.

ARTICLE ADDENDUM

Channels 5:2, 1-5; March/April 2011; © 2011 Landes Bioscience

Role of different voltage-gated Ca^{2+} channels in cortical spreading depression

Specific requirement of P/Q-type Ca^{2+} channels

Angelita Tottene, Andrea Urbani and Daniela Pietrobon*

Department of Biomedical Sciences; University of Padova; and CNR Institute of Neuroscience; Padova, Italy

Gain-of-function mutations in $Ca_V2.1$ (P/Q-type) Ca^{2+} channels cause familial hemiplegic migraine type 1 (FHM1), a subtype of migraine with aura. Knockin (KI) mice carrying FHM1 mutations show increased neuronal P/Q-type current and facilitation of induction and propagation of cortical spreading depression (CSD), the phenomenon that underlies migraine aura and may activate migraine headache mechanisms. We recently studied cortical neurotransmission in neuronal microcultures and brain slices of FHM1 KI mice, and showed (1) gain-of-function of excitatory neurotransmission, due to increased action potential-evoked Ca^{2+} influx and increased probability of glutamate release at pyramidal cell synapses, but unaltered inhibitory neurotransmission at fast-spiking interneuron synapses and (2) a causative link between enhanced glutamate release and facilitation of CSD induced by brief pulses of high K^+ in cortical slices.[1] Here, we show that after blockade of either the P/Q-type Ca^{2+} channels or the NMDA receptors, CSD cannot be induced in wild-type mouse cortical slices. In contrast, blockade of N- or R-type Ca^{2+} channels has only a small inhibitory effect on CSD threshold and velocity of propagation. Our findings support a model in which Ca^{2+} influx through presynaptic P/Q-type Ca^{2+} channels with consequent release of glutamate from recurrent cortical pyramidal cell synapses and activation of NMDA receptors are required for initiation and propagation of the CSD involved in migraine.

Key words: calcium channel, synaptic transmission, migraine, spreading depression, NMDA receptor, cortex

Submitted: 11/08/10

Accepted: 11/08/10

Previously published online: www.landesbioscience.com/journals/channels/article/14149

*Correspondence to: Daniela Pietrobon; Email: daniela.pietrobon@unipd.it

Addendum to: Tottene A, Conti R, Fabbro A, Vecchia D, Shapovalova M, Santello M, et al. Enhanced excitatory transmission at cortical synapses as the basis for facilitated spreading depression in $Ca_V2.1$ knockin migraine mice. Neuron 2009; 61:762–73; PMID: 19285472; DOI: 10.1016/j.neuron.2009.01.027.

Introduction

Missense mutations in the gene that encodes the pore-forming α_1 subunit of voltage-gated $Ca_V2.1$ (P/Q-type) Ca^{2+} channels cause a rare autosomal dominant subtype of migraine with aura: familial hemiplegic migraine type 1 (FHM1).[2] $Ca_V2.1$ channels are located in somatodendritic membranes and presynaptic terminals throughout the brain, and play a dominant role in initiating action potential-evoked neurotransmitter release at central nervous system synapses.[3] FHM1 mutations produce gain-of-function of human recombinant $Ca_V2.1$ channels, mainly due to a shift to lower voltages of channel activation.[4,5] Knockin (KI) mice carrying FHM1 mutations show increased P/Q-type Ca^{2+} current density in central neurons including cortical pyramidal cells.[1,6-8] Interestingly, the FHM1 KI mice also show a reduced threshold for induction of cortical spreading depression (CSD) and an increased velocity of propagation of CSD.[1,6,8] CSD can be induced in animals by focal stimulation of the cerebral cortex and consists in a slowly propagating wave of cortical neuronal and glial depolarization, whose mechanisms remain unclear and controversial.[9,10] Neuroimaging studies in humans indicate that CSD underlies the migraine aura; animal studies indicate that CSD may also trigger the migraine headache mechanisms.[11-13]

To study the cortical mechanisms that produce facilitation of CSD in FHM1 mutant mice, we investigated cortical neurotransmission in neuronal microcultures

and in brain slices from FHM1 KI mice.[1] The results show increased strength of excitatory synaptic transmission due to increased action potential-evoked Ca^{2+} influx through presynaptic P/Q-type Ca^{2+} channels and increased probability of glutamate release at cortical pyramidal cell synapses of mutant mice. In striking contrast, inhibitory neurotransmission at connected pairs of fast-spiking interneurons and pyramidal cells was unaltered in FHM1 mice, despite being initiated by P/Q-type Ca^{2+} channels.[1] To test the hypothesis that the gain-of-function of glutamate release at synapses onto pyramidal cells may explain the facilitation of induction and propagation of experimental CSD in FHM1 KI mice, we measured the threshold for CSD induction and the velocity of CSD propagation in acute slices of somatosensory cortex of R192Q KI mice before and after perfusion with a concentration of ωAgaIVA that reduced glutamate release at KI pyramidal cell synapses to wild-type (WT) levels. Strikingly, restoration of glutamate release to WT levels completely rescued CSD facilitation, as both CSD triggering threshold and CSD propagation rate in mutant mice became similar to those in WT mice.[1] This finding provides direct evidence of a causative link between enhanced glutamate release at pyramidal cell synapses and facilitation of experimental CSD, thus giving insights into the controversial mechanisms of CSD initiation and propagation. The initiation of the positive feedback cycle that ignites CSD and almost zeroes the neuronal membrane potential depends on the local increase of the extracellular concentration of K^+ ions $[K^+]_o$ above a critical value and on the activation of a net inward current at the pyramidal cell dendrites;[9] the nature of the cationic channels mediating this inward current remains unclear and controversial, although there is strong pharmacological support for a key role of NMDA receptors[9,10] (cf also Discussion and references therein). The findings of Tottene et al.[1] support a model of CSD initiation in which activation of presynaptic P/Q-type Ca^{2+} channels with consequent release of glutamate from recurrent cortical pyramidal cell synapses and activation of NMDA receptors (and possibly postsynaptic P/Q-type Ca^{2+} channels) are key components of the positive feedback cycle that ignites CSD in normally metabolizing cortical tissue. Regarding CSD propagation, the findings are consistent with a model based on interstitial K^+ diffusion initiating in adjacent dendrites this positive feedback cycle.[1]

Since it is controversial whether activation of NMDA receptors and in particular Ca^{2+} influx and synaptic transmission play only a modulatory role or are required for CSD induction and propagation,[9,10] we further investigated the role of NMDA receptors and of the different voltage-gated Ca^{2+} channel by studying the effect of specific blockers of these channels on the threshold for CSD induction and the velocity of CSD propagation in acute slices of mouse cerebral cortex.

Results

To investigate the role of the NMDA receptors and the P/Q-, N-, R- and L-type Ca^{2+} channels in initiation and propagation of experimental CSD, we measured the threshold for CSD induction and the velocity of CSD propagation, induced by brief pulses of high K^+ in acute slices of mouse somatosensory cortex, before and after application of saturating concentrations of D-AP5 (50 uM), ωAgaIVA (300 or 400 nM), ωCgTxGVIA (1 μM), SNX-482 (300 or 500 nM) and nimodipine (10 μM), respectively, as described in Tottene et al.[1] Pressure pulses of increasing duration were applied to a 3 M KCl-containing pipette positioned on layer 2/3 until a CSD was observed. CSD was revealed by both the associated changes in light transmittance and the typical depolarization to almost zero mV recorded in a pyramidal cell located 600 μm apart from the pressure-ejection pipette tip (to ensure that a true propagating event was studied). The duration of the first pulse eliciting a CSD was taken as CSD threshold, and the rate of horizontal spread of the change in intrinsic optical signal as velocity of CSD propagation.[1]

CSD could not be induced after blocking either the NMDA receptors or the P/Q-type Ca^{2+} channels; in fact, in the presence of either D-AP5 or ωAgaIVA, neither a depolarization of the patch-clamped pyramidal cell nor a propagating change in intrinsic optic signal were measured even with K^+ pulses 30 times longer than the threshold pulses triggering a CSD in control (**Table 1**). After the inhibition of P/Q-type Ca^{2+} channels, K^+ pulses of 10 s duration were unable to elicit a CSD in slices in which the average threshold duration in control was 0.29 ± 0.01 s (n = 7). Similarly, after the inhibition of NMDA receptors with D-AP5, K+ pulses of 10 s duration were unable to elicit a CSD in slices in which the average threshold duration in control was 0.34 ± 0.03 s (n = 5). Moreover, CSD was also not elicited in 9 (in the presence of ωAgaIVA) and 9 (in the presence of D-AP5) additional slices in which the maximal duration of the K^+ pulse was 1 s (about 3 times larger than the threshold in control) (**Table 1**).

In contrast, inhibition of the other types of presynaptic voltage gated Ca^{2+} channels had only a relatively small effect on CSD initiation and propagation. In the presence of either ωCgTxGVIA (n = 13) or SNX-482 (n = 10), the CSD threshold was about 10% higher and the CSD rate of propagation 15% lower than in control (**Fig. 1 and Table 1**). Neither threshold nor velocity of propagation of CSD was significantly affected by inhibition of L-type Ca^{2+} channels with nimodipine (n = 5) (**Table 1**).

Discussion

Our pharmacological study supports the conclusions that (1) Ca^{2+} influx through P/Q-type Ca^{2+} channels and activation of NMDA receptors are required for CSD induction by K^+ pressure pulses in acute slices of mouse sensory cortex; (2) Ca^{2+} influx through N- and, probably, R-type Ca^{2+} channels may play a modulatory role on CSD threshold and velocity of propagation.

In agreement with our findings, most previous studies investigating the effect of NMDA receptor antagonists on CSD, induced by brief K^+ pulses in cortical slices, reported complete blockade of CSD recorded at ≥500 um from the local K^+ ejection,[14-17] (but reviewed in ref. 18 for an exception in hippocampal slices); moreover CSD could not be recorded after perfusing the slices in Ca^{2+}-free medium or after blocking the Ca^{2+} channels with

Table 1. Effect of inhibition of the different types of voltage-gated Ca^{2+} channels or the NMDA receptors on CSD threshold and CSD velocity

		Control		Channel inhibition	
	n	Threshold (ms)	Velocity (mm/min)	Threshold (ms)	Velocity (mm/min)
ωAgaIVA	7	293 ± 12	2.3 ± 0.2	No CSD (10 s)	
	9	292 ± 7	2.1 ± 0.1	No CSD (1 s)	
D-AP5	5	338 ± 27	1.8 ± 0.1	No CSD (10 s)	
	9	286 ± 10	2.4 ± 0.1	No CSD (1 s)	
ωCgTxGVIA	13	261 ± 9	2.1 ± 0.1	284 ± 7 (***)	1.8 ± 0.1 (**)
SNX-482	10	288 ± 9	2.4 ± 0.2	317 ± 10 (**)	2.0 ± 0.1 (*)
Nimodipine	5	310 ± 21	2.2 ± 0.1	322 ± 19	2.1 ± 0.1

The threshold for CSD induction and the velocity of CSD propagation were measured before (control) and after (channel inhibition) application of saturating concentrations of D-AP5, ωAgaIVA, ωCgTxVIA, SNX-482 and nimodipine to inhibit NMDA receptors and P/Q-, N-, R- and L-type Ca^{2+} channels, respectively. CSD was induced in acute cortical slices by high K^+ pressure pulses of increasing duration: the duration of the first pulse eliciting a CSD was taken as CSD threshold and the rate of horizontal spread of the change in intrinsic optical signal as velocity of CSD propagation. In the presence of ωAgaIVA or D-AP5, the CSD could not be induced even with very long pulses, about 3 (1 s) or 30 (10 s) times larger than the control CSD triggering threshold.

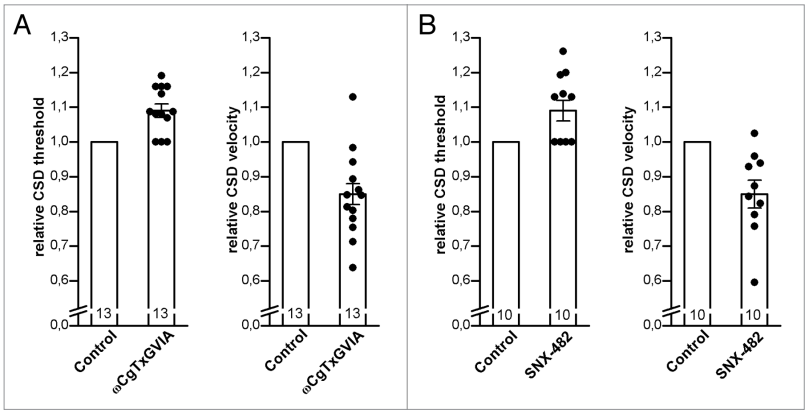

Figure 1. Relative values of CSD threshold and velocity before and after inhibition of N-type or R-type Ca^{2+} channels. The threshold for CSD induction and the velocity of CSD propagation were measured before (control) and after application of saturating concentrations of ωCgTxGVIA (A, n = 13) or SNX-482 (B, n = 10). The values obtained in the individual experiments in the presence of toxin relative to the corresponding control values are shown as dots and the average relative values as bar plots.

Cd^{2+},[14,16] or Ni^{2+} and Co^{2+}.[19] These findings are consistent with the conclusion that activation of NMDA receptors and Ca^{2+} influx through Ca_V channels are both required for CSD induction and/or propagation (although a possible caveat is the uncertainty regarding how much the K^+ stimulus exceeded the CSD threshold). Here, we have confirmed and extended the previous in vitro studies by showing that activation of P/Q-type Ca^{2+} channels is specifically required for induction of CSD by K^+ pulses, and that, after blockade of either the P/Q-type Ca^{2+} channels or the NMDA receptors, stimuli 30 times larger than the CSD threshold are unable to induce a CSD. Our findings in cortical slices are consistent with in vivo studies of CSD induced by electrical stimulation of the cortex, showing that, after i.p. injection of NMDA antagonists, even stimulation currents 10 times longer and 8 times larger than the CSD triggering threshold were unable to induce a CSD,[20] and spontaneous *cacna1a* mouse mutants, with mutations that produce partial loss-of-function of the P/Q-type Ca^{2+} channel, required an approximately 10 fold higher electrical stimulation intensity to evoke a CSD than wild-type mice.[21]

However, if one considers previous in vitro and in vivo pharmacological studies of CSD induced by perfusing the cortical slices or the cortex with a high K^+ solution (rather than with brief K^+ pulses or electrical stimulation) a completely different picture emerges: NMDA antagonists only slightly increase the CSD threshold without affecting its velocity;[17,22] similarly, blockade of the P/Q-type (or the N-type) Ca^{2+} channels hardly affects the CSD threshold obtained by perfusing cortical

slices with progressively increasing K^+ concentrations,[22] and removal of extracellular Ca^{2+} ions does not block CSD induced by perfusing the slices with a high K^+ solution for 80–90 s (but reduces to about half the rate of propagation).[23] Moreover, multiple CSDs induced in vivo by continuous K^+ microdialysis or topical application of a KCl cristal are strongly reduced in frequency but not completely suppressed by P/Q-type (or N-type) Ca^{2+} channel blockers[24] and by NMDA antagonists (that also reduce their amplitude and duration).[25,26] The Ca^{2+} channel blockers do not affect CSD induced by pinprick in vivo.[24,27]

Thus, even limiting our discussion to the methods that are used to elicit CSD in normally metabolizing cortical tissues (because the pharmacological profile of hypoxia and/or ouabain-induced CSD is again different), it is clear that different methods lead to different pharmacological profiles regarding the role of NMDA receptors and Ca^{2+} influx through P/Q-type Ca^{2+} channels in CSD induction and propagation. The different pharmacological profiles likely reflect the fact that CSD is a complex phenomenon and there may be sequential mechanisms with different pharmacology leading to the final common downstream CSD event;[10] some of the upstream mechanisms may be variably bypassed and/or occluded by the different CSD-inducing methods.

It becomes then crucial to understand which experimental CSD-inducing method is more relevant (and eventually most predictive of drug efficacy) for the CSDs that arise "spontaneously" in a given brain pathology.[12] In the case of migraine, insights into how "spontaneous" CSDs may arise have been provided by the interesting finding of enhanced excitatory neurotransmission at cortical pyramidal cell synapses but unaltered inhibitory neurotransmission at fast-spiking interneuron synapses in FHM1 KI mice.[1] A plausible working hypothesis is that the differential effect of FHM1 mutations on excitatory and inhibitory neurotransmission may, in certain conditions (cf migraine triggers), lead to disruption of the cortical excitation-inhibition balance due to excessive recurrent excitation, resulting in overexcitation and neuronal hyperactivity, that may increase $[K^+]_o$ above the critical value for CSD ignition.[28] Thus, to study mechanisms of experimental CSD that may be relevant to understand the mechanisms of the "spontaneous" CSD underlying migraine aura, electrical stimulation and/or brief applications of high K^+ appear as more appropriate CSD-inducing stimuli than prolonged applications of high K^+ and/or pinprick.

Our previous[1] and present findings support the idea that Ca^{2+} influx through presynaptic P/Q-type Ca^{2+} channels with consequent release of glutamate from recurrent cortical pyramidal cell synapses and activation of NMDA receptors are required for initiation and propagation of "spontaneous" CSDs in migraineurs. The specificity of the P/Q-type Ca^{2+} channel requirement compared to that of the other presynaptic N- and R-type Ca^{2+} channels may reflect the fact that excitatory synaptic transmission at pyramidal cell synapses in different areas of the cerebral cortex depends predominantly on P/Q-type Ca^{2+} channels (reviewed in ref. 28), and/or may point to a specific role of postsynaptic P/Q-type Ca^{2+} channels in CSD induction.

Acknowledgements

This work was supported by Telethon Italy (grant GGP06234), the Italian Ministry of University and Research (PRIN2007), the Fondazione CARIPARO (Calcium signalling in health and disease) and the University of Padova (Strategic project: Physiopathology of signalling in neuronal tissue).

References

1. Tottene A, Conti R, Fabbro A, Vecchia D, Shapovalova M, Santello M, et al. Enhanced excitatory transmission at cortical synapses as the basis for facilitated spreading depression in $Ca_v2.1$ Knockin migraine mice. Neuron 2009; 61:762-73.
2. Ophoff RA, Terwindt GM, Vergouwe MN, van Eijk R, Oefner PJ, Hoffman SMG, et al. Familial hemiplegic migraine and episodic ataxia type-2 are caused by mutations in the Ca^{2+} channel gene CACNL1A4. Cell 1996; 87:543-52.
3. Pietrobon D. Function and dysfunction of synaptic calcium channels: insights from mouse models. Curr Opin Neurobiol 2005; 15:257-65.
4. Pietrobon D. $Ca_v2.1$ channelopathies. Pflugers Arch 2010; 460:375-93.
5. Tottene A, Fellin T, Pagnutti S, Luvisetto S, Striessnig J, Fletcher C, et al. Familial hemiplegic migraine mutations increase Ca^{2+} influx through single human $Ca_v2.1$ channels and decrease maximal $Ca_v2.1$ current density in neurons. PNAS 2002; 99:13284-9.
6. van den Maagdenberg AM, Pietrobon D, Pizzorusso T, Kaja S, Broos LA, Cesetti T, et al. A Cacna1a knockin migraine mouse model with increased susceptibility to cortical spreading depression. Neuron 2004; 41:701-10.
7. Inchauspe CG, Urbano FJ, Di Guilmi MN, Forsythe ID, Ferrari MD, van den Maagdenberg AM, et al. Gain of function in FHM-1 $Ca_v2.1$ knock-in mice is related to the shape of the action potential. J Neurophysiol 2010; 104:291-9.
8. van den Maagdenberg AM, Pizzorusso T, Kaja S, Terpolilli N, Shapovalova M, Hoebeek FE, et al. High cortical spreading depression susceptibility and migraine-associated symptoms in $Ca_v2.1$ S218L mice. Ann Neurol 2010; 67:85-98.
9. Somjen GG. Mechanisms of spreading depression and hypoxic spreading depression-like depolarization. Physiol Rev 2001; 81:1065-96.
10. Charles A, Brennan K. Cortical spreading depression-new insights and persistent questions. Cephalalgia 2009; 29:1115-24.
11. Pietrobon D, Striessnig J. Neurobiology of migraine. Nat Rev Neurosci 2003; 4:386-98.
12. Ayata C. Spreading depression: from serendipity to targeted therapy in migraine prophylaxis. Cephalalgia 2009; 29:1095-114.
13. Zhang X, Levy D, Noseda R, Kainz V, Jakubowski M, Burstein R. Activation of meningeal nociceptors by cortical spreading depression: implications for migraine with aura. J Neurosci 2010; 30:8807-14.
14. Footitt DR, Newberry NR. Cortical spreading depression induces an LTP-like effect in rat neocortex in vitro. Brain Res 1998; 781:339-42.
15. Vilagi I, Klapka N, Luhmann HJ. Optical recording of spreading depression in rat neocortical slices. Brain Res 2001; 898:288-96.
16. Peters O, Schipke CG, Hashimoto Y, Kettenmann H. Different mechanisms promote astrocyte Ca^{2+} waves and spreading depression in the mouse neocortex. J Neurosci 2003; 23:9888-96.
17. Petzold GC, Windmuller O, Haack S, Major S, Buchheim K, Megow D, et al. Increased extracellular K^+ concentration reduces the efficacy of N-methyl-D-aspartate receptor antagonists to block spreading depression-like depolarizations and spreading ischemia. Stroke 2005; 36:1270-7.
18. Larrosa B, Pastor J, Lopez-Aguado L, Herreras O. A role for glutamate and glia in the fast network oscillations preceding spreading depression. Neuroscience 2006; 141:1057-68.
19. Jing J, Aitken PG, Somjen GG. Role of calcium channels in spreading depression in rat hippocampal slices. Brain Res 1993; 604:251-9.
20. Marrannes R, Willems R, De Prins E, Wauquier A. Evidence for a role of the N-methyl-D-aspartate (NMDA) receptor in cortical spreading depression in the rat. Brain Res 1988; 457:226-40.
21. Ayata C, Shimizu-Sasamata M, Lo EH, Noebels JL, Moskowitz. Impaired neurotransmitter release and elevated threshold for cortical spreading depression in mice with mutations in the α_{1A} subunit of P/Q type calcium channels. Neuroscience 2000; 95:639-45.
22. Petzold GC, Haack S, von Bohlen Und Halbach O, Priller J, Lehmann TN, Heinemann U, et al. Nitric oxide modulates spreading depolarization threshold in the human and rodent cortex. Stroke 2008; 39:1292-9.
23. Zhou N, Gordon GR, Feighan D, MacVicar BA. Transient swelling, acidification, and mitochondrial depolarization occurs in neurons but not astrocytes during spreading depression. Cereb Cortex 2010; 20:2614-24.
24. Richter F, Ebersberger A, Schaible HG. Blockade of voltage-gated calcium channels in rat inhibits repetitive cortical spreading depression. Neurosci Lett 2002; 334:123-6.

25. Herreras O, Somjen GG. Analysis of potential shifts associated with recurrent spreading depression and prolonged unstable SD induced by microdyalisis of elevated K^+ in hippocampus of anesthetized rats. Brain Res 1993; 610:283-94.
26. Peeters M, Gunthorpe MJ, Strijbos LM, Goldsmith P, Upton N, James MF. Effects of pan-and subtype-selective N-Methyl-D-aspartate receptor antagonists on cortical spreading depression in the rat: therapeutic potential for migraine. J Pharmacol Exp Ther 2007; 321:564-72.
27. Akerman S, Holland PR, Goadsby PJ. Mechanically-induced cortical spreading depression associated regional cerebral blood flow changes are blocked by Na^+ ion channel blockade. Brain Res 2008; 1229:27-36.
28. Pietrobon D. Insights into migraine mechanisms and $Ca_V2.1$ calcium channel function from mouse models of familial hemiplegic migraine. J Physiol 2010; 588:1871-8.

4. Results (Ib)

NMDA receptors inhibition in FHM1 R192Q KI mice does not block CSD induction and propagation

After the demonstration of a key role of both P/Q-type Ca^{2+} channels and NMDA receptors in WT mice, I focused my work on the FHM1 R192Q KI mouse. Slices from the somatosensory cortex of these mice exhibited an increased action potential-mediated Ca^{2+} influx through P/Q-type Ca^{2+} channels and an increased glutamate release at cortical pyramidal synapses. To investigate the role of NMDA receptors in CSD induction and propagation in these mice, CSD threshold and velocity were measured before and after 50 µM D-AP5 application, using the protocol described in Tottene et al., 2011 (pdf attached in chapter 3). In contrast to results obtained in slices from WT mice, in KI slices NMDA receptor inhibition failed to block CSD induction and propagation and only increased CSD threshold (90 ± 9%, n = 14) and decreased CSD velocity (47 ± 1%; n = 13) (Figure 4.1).

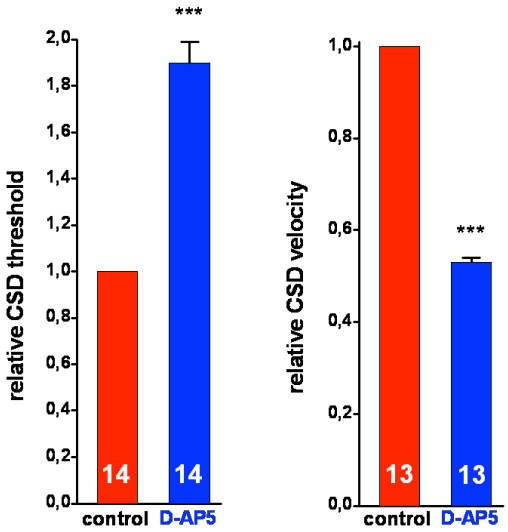

Figure 4.1: NMDA receptors block in FHM1 R192Q KI mice increases CSD threshold and decreases CSD velocity

Left: Average relative CSD threshold from 14 experiments before (control) and after application of D-AP5 (50 µM). Relative CSD threshold is expressed as the ratio between CSD threshold in the presence of D-AP5 and control threshold.

Right: Average relative CSD velocity from 13 experiments before and after application of D-AP5 (50 µM).

Further experiments demonstrated that also higher concentrations of D-AP5 (100 and 200 µM) did not block CSD induction and propagation in KI mice (see chapter 5, Discussion).

5. Discussion (I)

To gain insights into the mechanism of CSD induction and propagation I measured in acute cortical slices from WT and FHM1 R192Q KI mice CSD threshold and velocity in presence or absence of specific blockers of voltage-gated Ca^{2+} channel and NMDA receptors. CSD was induced by different duration pressure pulses applied to a KCl-containing glass pipette until a CSD was detected. The duration of the first pulse inducing a CSD was taken as CSD threshold, while CSD velocity was calculated as the rate of IOS signal propagation on the slice surface.

Results from WT mice demonstrated a necessary role of P/Q-type Ca^{2+} channels and NMDA receptors, while other types of voltage-gated Ca^{2+} channels appeared to be little or not involved. Our findings are in agreement with the CSD model proposed by Pietrobon (2007). In this model stimuli that induce a CSD upon the increase in [K+]out, are accompanied by sustained neuronal depolarization and intense firing that overwhelm the regulatory mechanisms that normally keep [K+]out within the physiological range.. In this model P/Q-type Ca^{2+} channels play a necessary role because after their specific block, application of KCl stimuli up even 30 fold longer duration than that in controls fails to induce a CSD . In striking contrast, blockage of N- and R-type voltage-gated Ca^{2+} channels led only to a slightly increase in CSD induction threshold and a slightly decrease in CSD propagation velocity. The specific requirement of the P/Q-type Ca^{2+} channel compared to that of the other presynaptic voltage-gated Ca^{2+} channels may have two non-mutually excluding explanations: i) the excitatory synaptic transmission at pyramidal cell synapses in different areas of the cerebral cortex depends predominantly on P/Q-type Ca^{2+} channels (reviewed in Pietrobon, 2010) and ii) postsynaptic P/Q-type Ca^{2+} channels play a specific role of in CSD induction.

In contrast to result obtained from WT mice in which in presence of 50 μM D-AP5 stimuli up to 30 times the control threshold failed to induce a CSD, NMDA receptors inhibition in FHM1 R192Q mice did not lead to CSD suppression. Notably, D-AP5 in KI mice led to a significant increase in CSD induction threshold and a significantly decrease in CSD propagation velocity. Indeed, both CSD threshold and velocity are almost doubled. The substantial difference between the inhibition of CSD generation in WT mice and the partial inhibition observed in KI mice may be due to two different factors: i) D–AP5 was used at concentrations that could not fully antagonize the action of glutamate, at least in R192Q KI mice. Notably, in R192Q KI mice the release of glutamate at cortical pyramidal neuron synapses is increased and D-AP5 is a competitive NMDA receptor antagonist (Tottene et al., 2009); ii) in R192Q KI mice CSD generation is governed also by additional elements that are not described in our CSD model. This challenging hypothesis may be in accordance with the release of other

excitatory neurotransmitters and/or with a specific role of postsynaptic P/Q-type Ca^{2+} channels.

In a few additional experiments we observed that even higher concentrations of D-AP5 (100 and 200 μM) failed to block CSD induction. Given the low number of experiments (n = 4), additional experiments are need to obtain a precise quantification of the effect of 100-200 μM D-AP5 on the CSD threshold.

An additional experiment that could help to clarify this issue is to measure CSD threshold and velocity before and after the application of a non-competitive NMDA inhibitor such as MK-801.

6. Aim of work (II)

Previously shown results demonstrated that P/Q type Ca^{2+} channels and NMDA receptors are required for CSD induction and propagation in WT mice. In spite of this other elements may be involved in the positive-feedback cycle igniting CSD.

Over the last decade astrocytes were revealed to play important roles in brain function. Astrocytes activated by synaptic neurotransmitters can signal back to neurons by releasing various gliotransmitters that modulate neuronal excitability and synaptic transmission. Among these gliotransmitters, glutamate was revealed to specifically act on extrasynaptic NMDA receptors and favor neuronal synchronies. On the basis of these observations, the hypothesis that neuron-astrocyte crosstalk may be involved in CSD initiation and propagation was tested.

Devices used to study CSD mechanisms (i.e. patch clamp recordings and Ca^{2+} imaging) allowed to observe cortical spontaneous activity in neurons from neocortical slices. Indeed, neurons exhibited sustained increases of their cytosolic Ca^{2+} signal that in simultaneous current clamp recordings coincided with up-states. Because cortical astrocytes also exhibited spontaneous Ca^{2+} elevations, we advanced the hypothesis that these cells contribute to regulate the up- and down-states that characterize spontaneous activities in the neuronal network.

7. Results (II)

7.1 Sub-threshold depolarizations and CSD are characterized by different phases

To further investigate the mechanisms underlying CSD induction and propagation, pyramidal cells located at approximately 100 and 200 μm from the KCl application site were patched while KCl stimuli of increasing duration were applied until a CSD was observed. Current-clamp recordings revealed that after both sub-threshold depolarizations and CSDs, individual neurons exhibited a depolarization characterized by three distinct peaks. The first two peaks were present in the response evoked by both sub-threshold stimuli and stimuli that evoked a CSD. In contrast, the third peak was specifically linked to CSD. Lower sub-threshold depolarizations were characterized by a rapid phase and a single noisy peak which increased in amplitude in parallel to the increasing KCl pulse intensity. Stronger KCl stimulations induced depolarizations that showed a second, less noisy peak with an amplitude which was also dependent on stimulus intensity. In pyramidal cells at 200 μm from the KCl application site, it was often difficult to distinguish the two peaks; however depolarizations recorded at this distance showed smaller amplitude and slower kinetics. After a KCl stimulation that evoked a CSD, the rapid phase and the first two peaks, followed by the CSD-specific third peak to almost 0 mV, were clearly detectable (Figure 7.1).

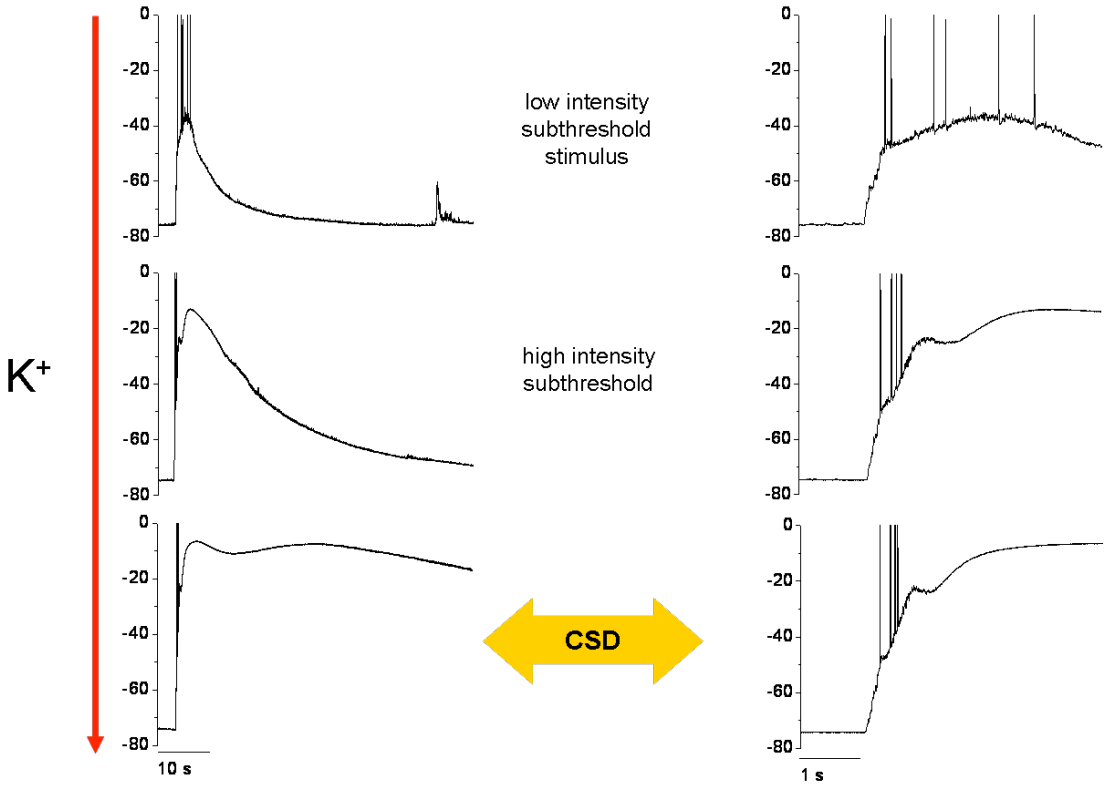

Figure 7.1 Different phases of voltage changes with increasing intensity of (sub-threshold and threshold) KCl stimuli at different distance from KCl-injecting pipette

Current-clamp recordings from a layer 2-3 pyramidal cell located at 100 µm afar from KCl-injecting pipette. From the top: a low intensity sub-threshold stimulus, a high intensity sub-threshold stimulus and a CSD.

Left: A compressed time scale allows to observe that the low intensity stimulus is characterized by a rapid depolarization phase ending in a single noisy peak with firing, while the high intensity one present also a second, less noisy, peak. CSD includes an additional third peak, with amplitude similar to the second one.

Right: A more expanded time scale allows to observe the complex kinetics of different voltage phases. Note the presence of a rapid phase with firing, ending in a noisy peak in both sub-threshold depolarizations and CSD. This time scale allows to observe the transition between the first and the second, less noisy, peak.

Patch-clamp experiments allowed a highly accurate description of sub-threshold depolarizations and CSD in individual neurons, but they can not provide information on both the level of neuronal synchrony in the network and the spatial-temporal features of CSD propagation. Some insights into these important aspects in CSD induction and propagation can be obtained by utilizing laser scanning microscope Ca^{2+} imaging techniques. The Ca^{2+} signal has been, indeed, shown to increase in neurons in strict accordance with the action potential discharges. By visualizing in brain slice preparations the Ca^{2+} signal from tens of neurons located at different distances from the KCl-injection site, we can, therefore, follow how a focally evoked CSD can propagate across the neuronal network (Figure 7.2).

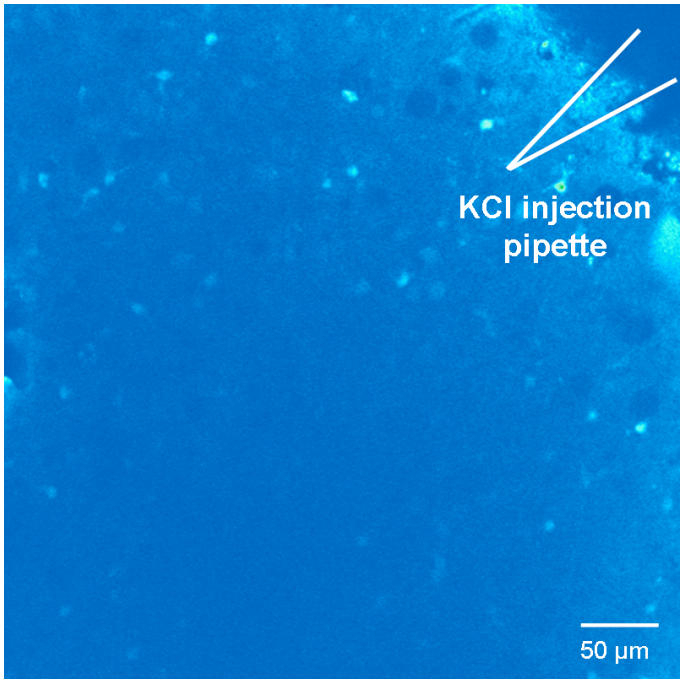

Figure 7.2 Example of the optical field during confocal scanning of a cortical slice loaded with the Ca^{2+}-sensitive dye OGB1-AM

To compare the membrane potential variations in individual pyramidal neurons and Ca^{2+} changes in the neuronal network I also performed patch-clamp recordings and simultaneous Ca^{2+} imaging. As expected, a strict correlation was observed between the current clamp trace and the neuronal Ca^{2+} signal (Figure 7.3).

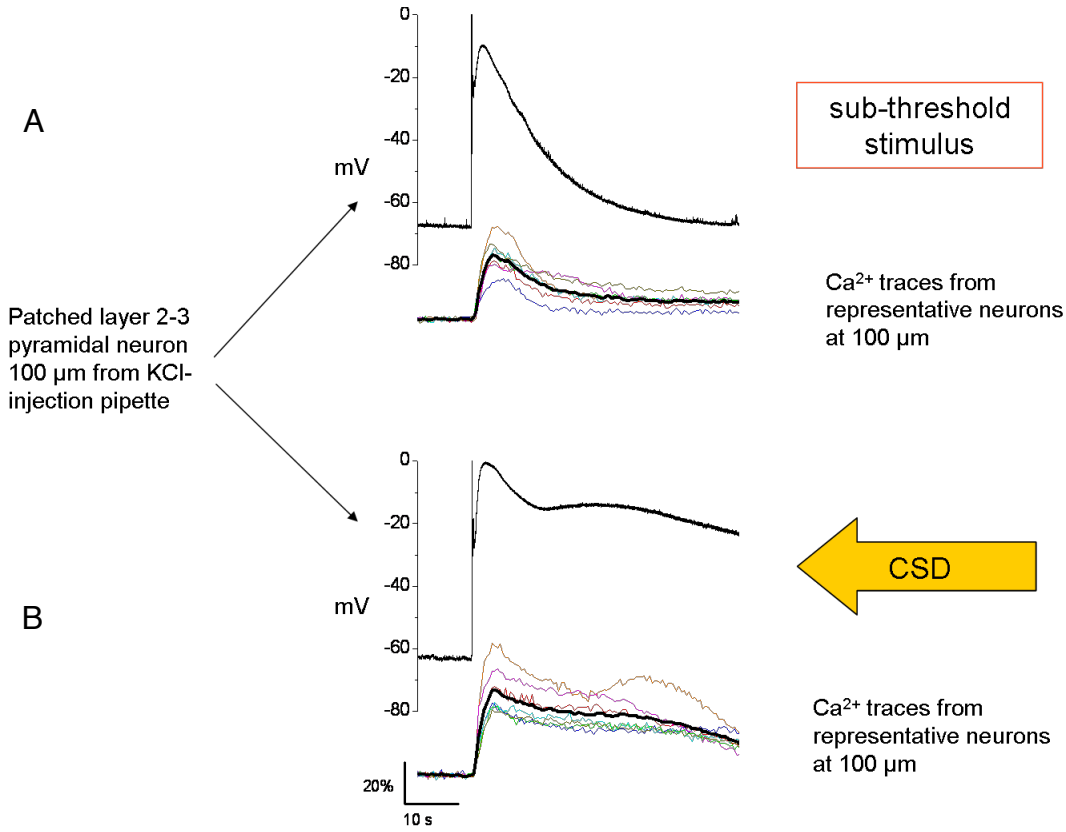

Figure 7.3: Correlation between simultaneously acquired Ca^{2+} transients from neurons at 100 µm and current recordings from a pyramidal cell at 100 µm from the KCl-injecting pipette
A: Sub-threshold stimulus eliciting the typical rapid phase and the two peaks detectable at 100 µm and a single Ca^{2+} peak, corresponding to the second voltage peak.
B: CSD comprehends the rapid depolarization phase, the first and the second peak and the third, CSD-characterizing peak; simultaneous Ca^{2+} rises in other neurons present a first peak corresponding to the second voltage peak, and a prolonged flat phase corresponding to the third voltage peak.

The amplitude of neuronal Ca^{2+} increases evoked by sub-threshold stimuli increased in parallel with an increased intensity of KCl stimulation and decreased as a function of the distance from the KCl application site. Upon stimuli that evoked a CSD, the neuronal Ca^{2+} increase was of larger amplitude and it was characterized by two peaks. The first Ca^{2+} peak decreased with the distance from the KCl application site, similarly to the Ca^{2+} elevation evoked by a sub-threshold stimulation. In contrast, the second Ca^{2+} peak, which reflects a propagating CSD, remained unchanged at different distances from the stimulation site (Figure 7.4).

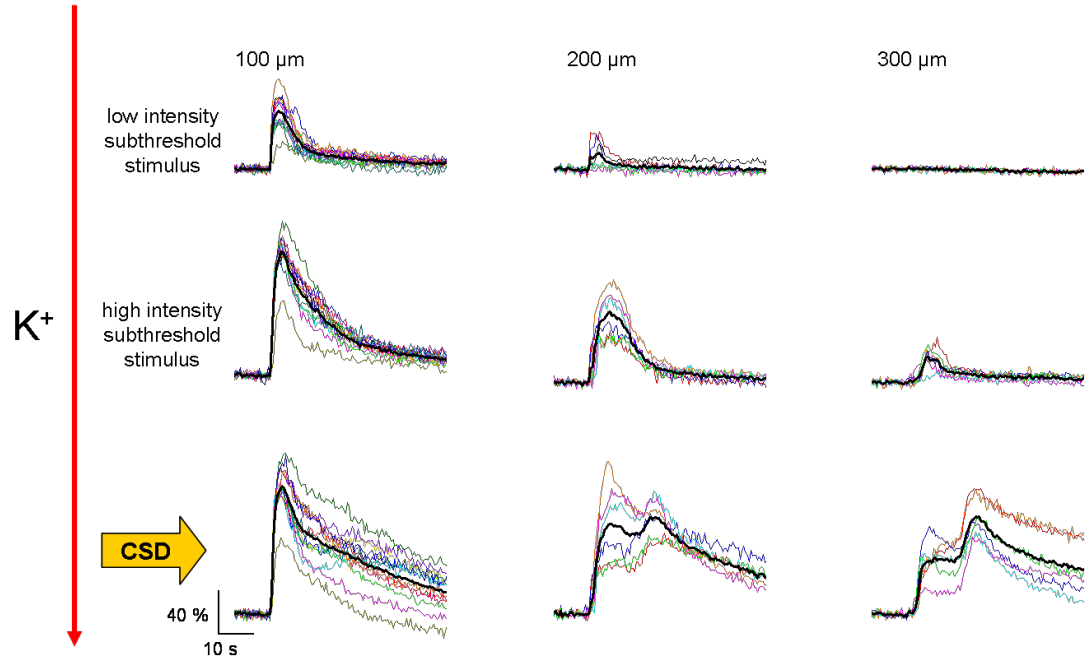

Figure 7.4: Different phases of Ca^{2+} neuronal increases induced by sub-threshold stimuli and CSD in OG-loaded brain slices

Fluorescence peaks, corresponding to intracellular Ca^{2+} increases, from individual neurons located at several distances (top, 100 µm; central, 200 µm; bottom, 300 µm) from the KCl injecting pipette. Colored traced represent normalized Ca^{2+} signals from individual neurons; black thicker traces represent the mean of all traces. All recordings were made during a single representative experiment.

Neuronal Ca^{2+} increases produced by sub-threshold stimuli are characterized by a single peak whose amplitude increases with the stimulus intensity and decreases with the distance from the KCl-injecting pipette. CSD is characterized by a first peak whose amplitude decreases with the distance, and a second one whose amplitude does not vary in function of distance.

Noteworthy is that sub-threshold KCl stimulations of increasing intensity activated an increasing number of neurons, until all neurons viable in the observation field were recruited into the propagating CSD (Figure 7.5).

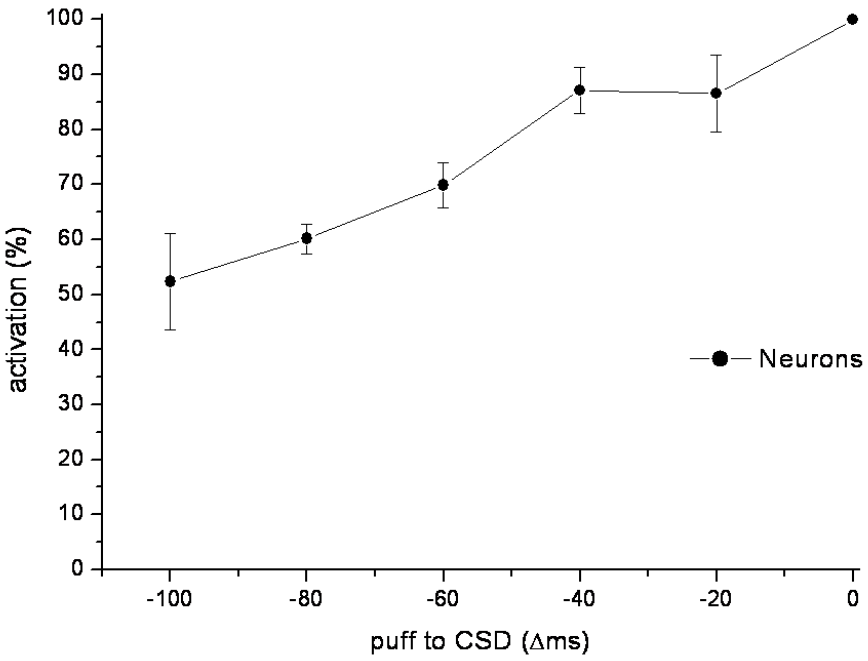

Figure 7.5: Fraction of active neurons increases with increasing intensity of KCl stimulus
Percentage of active neurons normalized to the maximal number of active neurons (detectable during CSD) as a function of the difference between stimulus duration and the CSD-inducing stimulus duration (indicated as 0). n = 4 experiments from 3 animals. 98 neurons per experiment (mean) were detectable in the observation field and were analyzed.

7.2 Role of neuron-astrocyte crosstalk in CSD induction and propagation

In our Ca^{2+} imaging experiments Ca^{2+} signals could be visualized from both neurons and astrocytes. Beside the smaller soma and a higher basal fluorescence level, astrocytes could be distinguished from neurons after slice incubation with both the Ca^{2+} dye Fluo4-AM and the astrocytes-selective morphological dye SR101 (n = 5) (Figure 7.6).

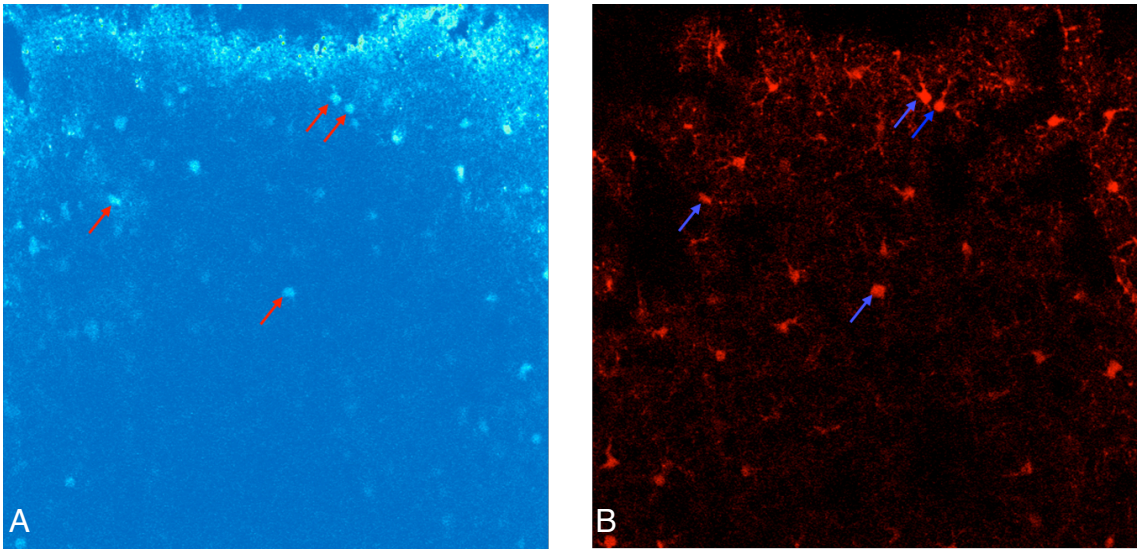

Figure 7.6: Simultaneous slices loading with the Ca^{2+}-sensitive dye Fluo-4 and the morphological astrocytic-selective dye SR101

A: Slice imaged with a 488 nm laser for Fluo-4. Red arrows point to example astrocytes.

B: Slice imaged with a 543 nm laser for SR101. Blue arrows point to example astrocytes. Note the correspondence between red arrows in A and blue ones in B.

I observed that KCl stimuli induced large amplitude Ca^{2+} elevations in astrocytes. Astrocytic Ca^{2+} increases induced by KCl stimuli varied greatly in different astrocytes, but in most astrocytes was composed also by long lasting Ca^{2+} oscillations that followed to the first Ca^{2+} increase triggered by KCl (Figure 7.7, 7.9).

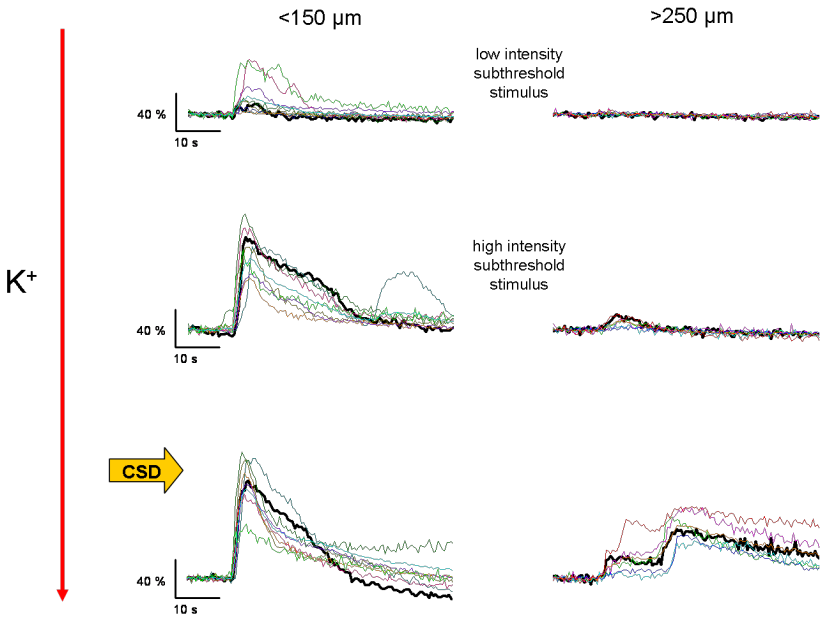

Figure 7.7: Astrocytic Ca^{2+} responses after KCl pulses

Colored traced represent normalized Ca^{2+} signals from individual astrocytes; black thicker traces represent the mean of all traces. All recordings were made during a single representative experiment.

Left: Ca^{2+} rises in astrocytes located near the KCl-injecting pipette (distance less than 150 µm). Note an additional Ca^{2+} oscillation following the direct response after applying an high intensity sub-threshold stimulus.

Right: Ca^{2+} rises in astrocytes located far from the KCl-injecting pipette (distance greater than 250 µm). No response is detectable after a low intensity sub-threshold stimulus and only a small one can be observed after an high intensity one. CSD is characterized by a first small direct response and an additional CSD-specific peak.

Sub-threshold KCl stimuli of increasing intensity induced both direct and oscillatory Ca^{2+} rises in an increasing number of astrocytes. As in the case of neurons, this number was initially low but it rapidly increased in parallel to the increased stimulus intensity, until almost all astrocytes were activated during a CSD (94.8 ± 4.4%, n = 4 experiments from 3 animals). (Figure 7.8) The amplitude of these Ca^{2+} elevations also increased in parallel with the increased stimulus intensity (Figure 7.7).

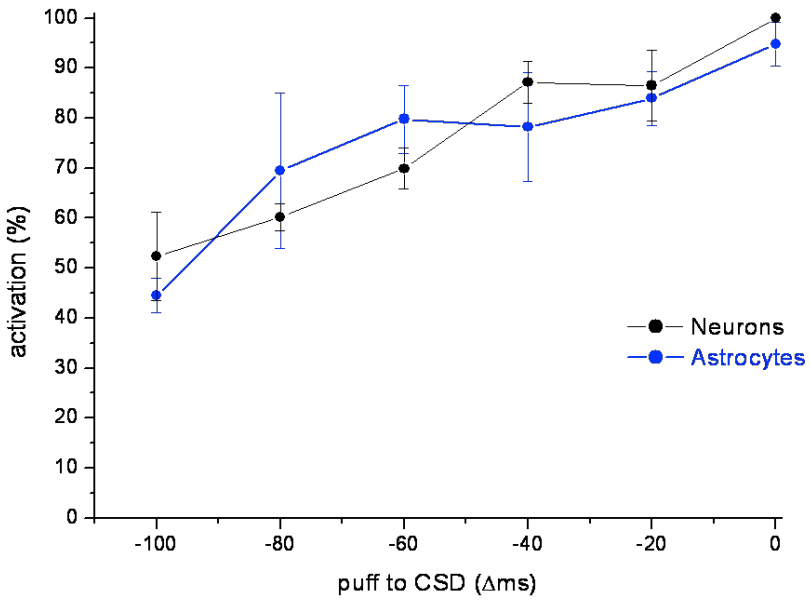

Figure 7.8: Fraction of active neurons and astrocytes increases with increasing intensity of KCl stimulus

Percentage of active neurons and astrocytes normalized to the maximal number of active ones as a function of stimulus duration difference to threshold, CSD-inducing, stimulus duration (indicated as 0). Maximal number of active astrocytes is calculated counting the active astrocytes in the observation field during an experiment: in fact not all astrocytes are active at the same time, not even during a CSD (indeed the maximal activation percentage, during CSD, is not 100%). n = 4 experiments from 3 animals. 98 neurons and 30 astrocytes per experiment (mean) were detectable in the observation field and were analyzed.

To clarify whether astrocytes could be involved in CSD induction and propagation, stimulation-induced astrocytic activation was blocked by slice perfusion with CPA, i.e., a SERCA inhibitor that deplete astrocytic internal Ca^{2+} stores. After CPA both direct and oscillatory astrocytic Ca^{2+} responses to both sub-threshold stimuli and CSD were blocked (Figure 7.9).

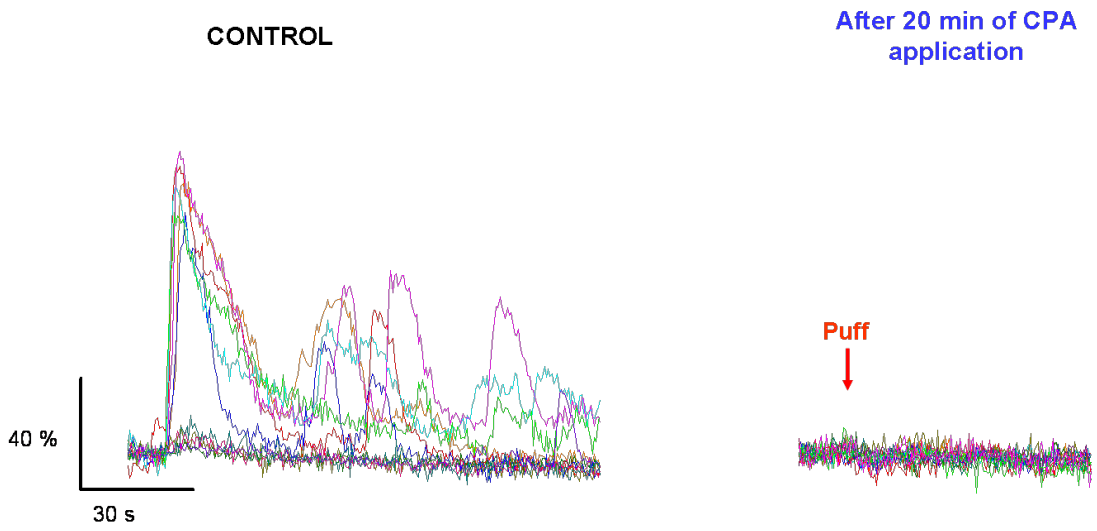

Figure 7.9: CPA application suppress KCl-induced astrocytic Ca^{2+} rises
Ca^{2+} traces from all astrocytes in the observation field before (control) and after application of 50 µm CPA; the same stimulus intensity was applied in both cases. Note the intense Ca^{2+} oscillations following the direct response in control.

Under these conditions, however, both amplitude and kinetics of neuronal responses to KCl stimuli were not significantly affected (Figure 7.10).

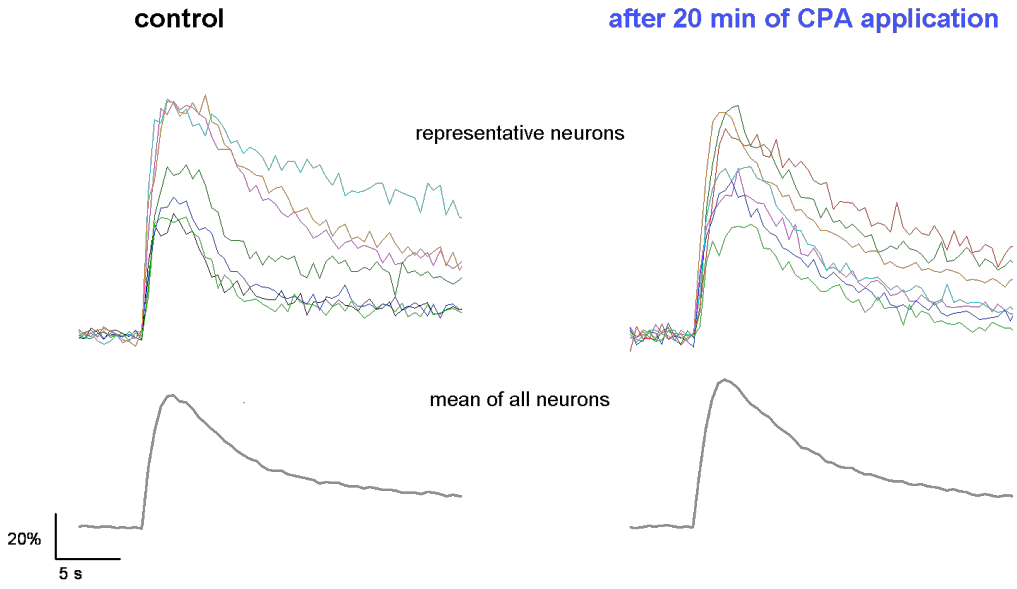

Figure 7.10: CPA application does not affect neuronal response to KCl stimuli
Colored traces depict representative traces from 7 on 87 active neurons in a observation field (from a single representative experiment) after a sub-threshold KCl stimulus; grey thicker traces below depict the mean of all 87 active neurons. A sub-threshold stimulus was applied before (control) and after CPA application for 20 minutes.

CSD threshold and velocity in brain slices from both WT and FHM1 KI mice, before and after CPA application, were also measured. CPA application did not significantly affect either CSD threshold or velocity in both WT and KI mice. Indeed, in WT mice CSD threshold and velocity in the presence of CPA were respectively 92 ± 4% (n = 6, p = 0.08) and 102 ± 5% (n = 6, p = 0.78) of control; in KI CSD threshold and velocity in the presence of CPA were 102 ± 7% (n = 6, p = 0.64) and 92 ± 6% (n = 6, p = 0.27) of control (Figure 7.11).

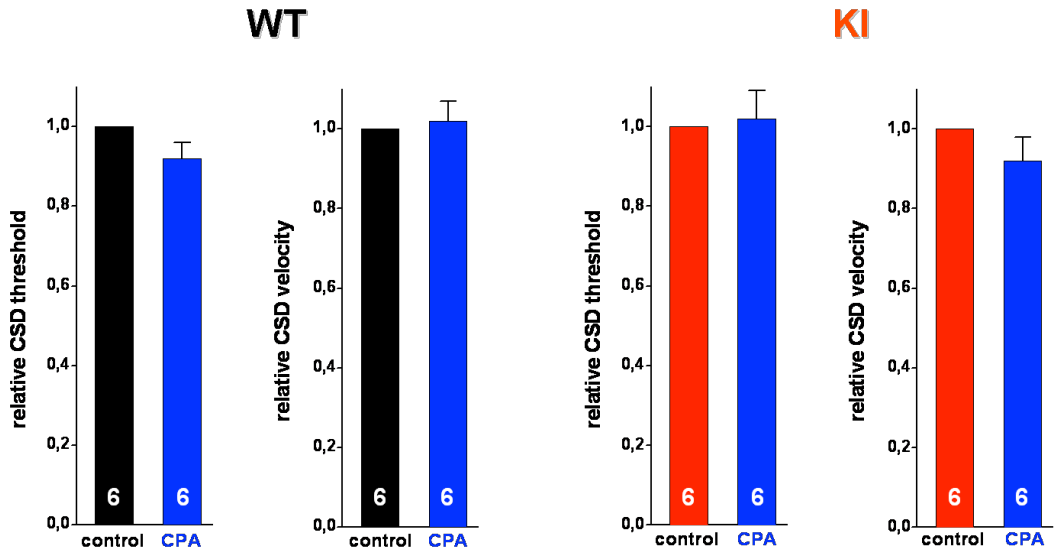

Figure 7.11: CPA application does not affect CSD threshold or CSD velocity
Left: Average relative CSD threshold and velocity from 6 experiments before (control) and after application of CPA (50 µM) in WT mice. Relative CSD parameters are expressed as the ratio between CSD parameter in the presence of CPA and control parameter.
Right: Average relative CSD threshold and velocity from 6 experiments before (control) and after application of CPA (50 µM) in FHM1 R192Q KI mice.

7.3 Neuron-astrocyte reciprocal signaling may contribute to spontaneous neuronal activities

Ca^{2+} imaging allowed to observe spontaneous Ca^{2+} elevations in neurons with a frequency of about 2 oscillations per minutes (Figure 7.12). This pattern of activity resembles the spontaneous up- and down states that can be observed in patch-clamp recordings from individual neurons in cortical slices (1.55 ± 0.10 min-1 in WT mice, Pietrobon, unpublished data). During some CPA experiments, it has been collaterally observed a modification of the spontaneous neuronal activities. This observation hints at a possible role of neuron-astrocyte cross-talk in spontaneous cortical activities. To check this possibility some preliminary experiments were performed.

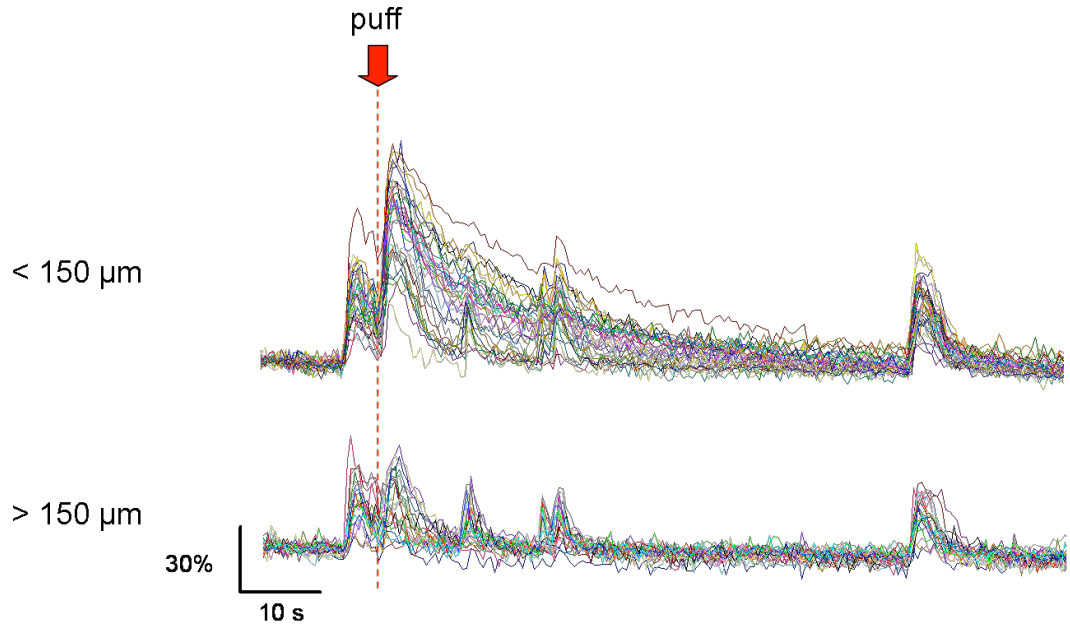

Figure 7.12: In some Ca^{2+} traces it is possible to distinguish some spontaneous activity

Top: Representative Ca^{2+} traces from neurons located close to the KCl-injecting pipette (distance <150 µM) show direct response to the stimulus and other synchronous oscillations.

Bottom: In neurons located far from the KCl-injecting pipette (distance > 150 µM), where KCl stimulus does not induce any neuronal response, it is still possible to detect the same synchronous oscillations observed in the traces above. Note that the synchronicity is conserved between the two groups of neurons.

7.3.1 General features of cortical spontaneous activity

In the absence of external stimulation a spontaneous slow oscillatory activities has been observed in neurons by both current-clamp recordings and Ca2+ imaging. Current clamp recordings allowed to detect slow oscillations in individual pyramidal cells in the cortical layer 2-3. These recordings confirmed the well known, but not yet well characterized, phenomenon in which periods of relatively low activities (down-states) alternate to periods of intense activities, with depolarization and firing in neurons (up-states) (Figure 7.13, 7.14A top).

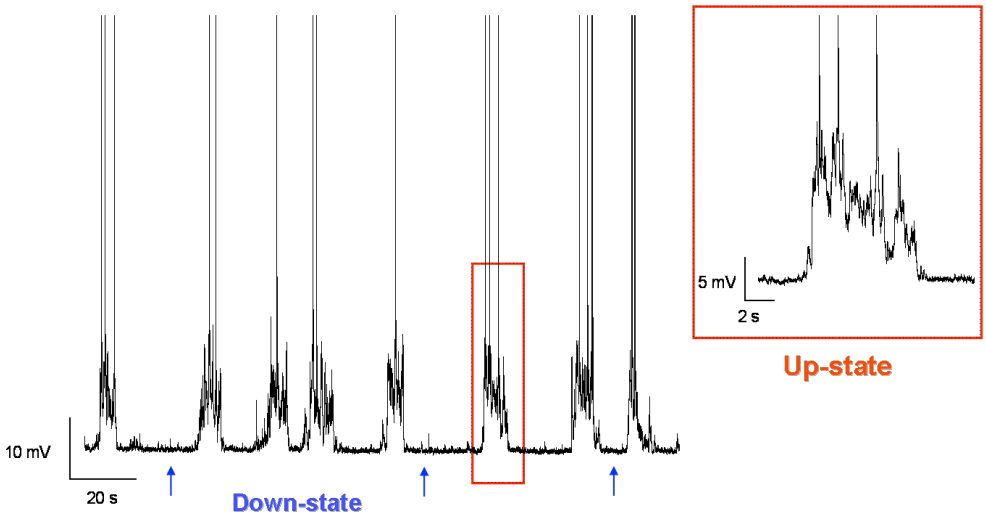

Figure 7.13: Representative current-clamp trace from a layer 2-3 pyramidal cell showing up- and down-states spontaneous activity

Inset: Representative up-state.

Blue arrows point examples of down-states in the trace.

Patch-clamp recordings allowed a very accurate description of the neuronal spontaneous activities with a high temporal gain, but were limited to one cell. Simultaneous patch-clamp and Ca2+ imaging of Fluo4-AM loaded brain slices allowed to observe in a number of neurons, in the absence of external stimuli, highly synchronous Ca2+ oscillations that may correspond to the up-states observed in the patched pyramidal neurons (Figure 7.14A).

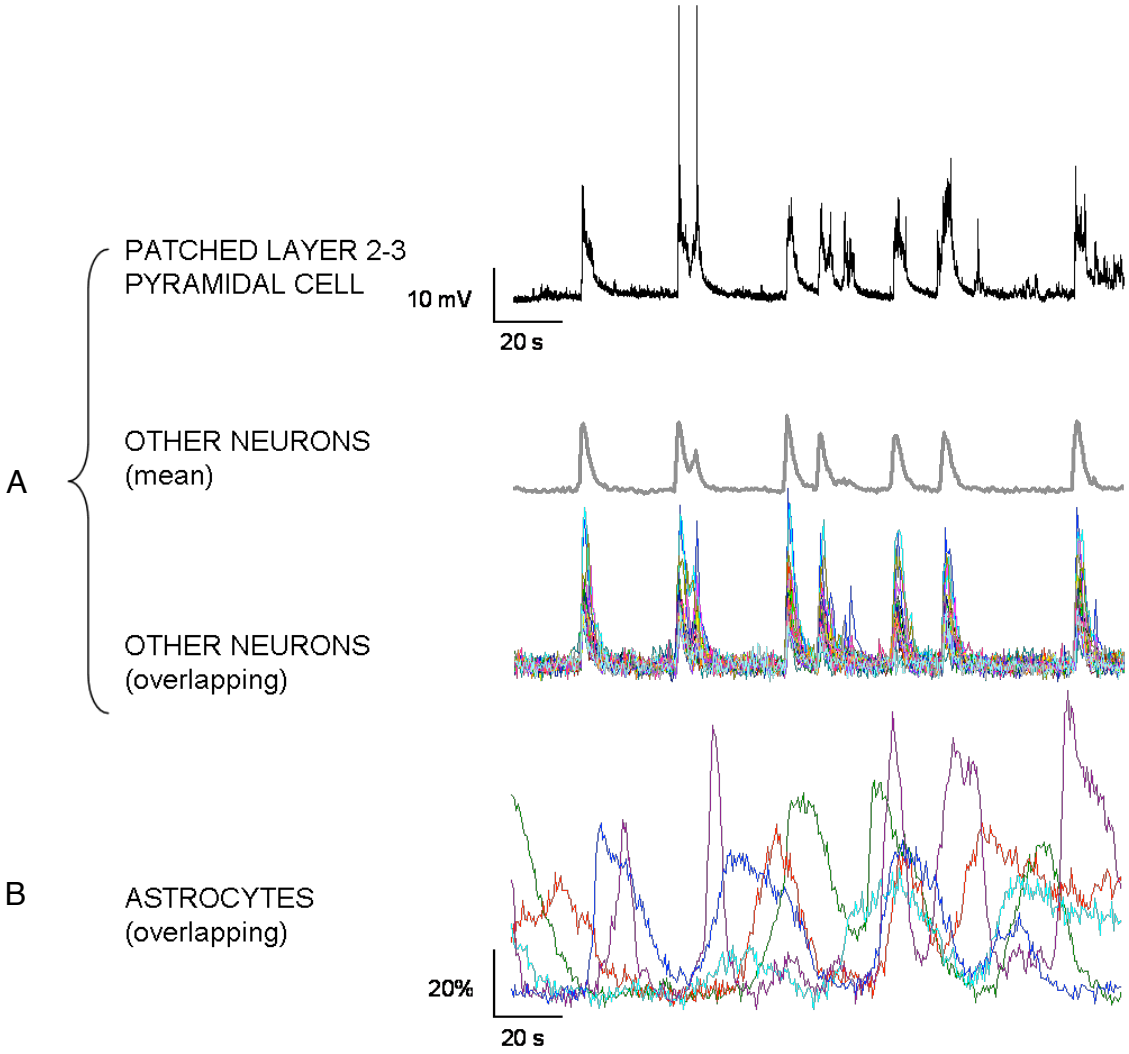

Figure 7.14: Spontaneous neuronal and astrocytic activity can be dissected by simultaneous patch-clamp and Ca^{2+} imaging in brain slices loaded with Fluo-4

A: Current clamp recording from a layer 2-3 pyramidal cell (top) allows to detect neuronal spontaneous up- and down-states. Current clamp recording is compared with Ca^{2+} traces from other neurons in the observation field. Colored traces represent individual neurons, while the grey thicker one represent the mean of all neurons. Note the correlation between Ca^{2+} traces and patch-clamp recording.

B: Ca^{2+} traces from representative astrocytes showing spontaneous asynchronous oscillations that apparently do not correlate with neuronal up- and down-states cycles.

In the absence of external stimulation a spontaneous astrocytic activity was also detected. Given the low frequency of neuronal spontaneous oscillations, to obtain an accurate evaluation of this activity, it was necessary to monitor the Ca^{2+} signal for long periods (ten to twenty minutes). To avoid photobleaching and photo-damage to neurons, a low-invasive protocol for Ca2+ imaging was developed. In this proticol, cortical slices were loaded with the Ca^{2+}-sensitive dye Fluo4-AM - that has an higher dynamic range than Oregon Green – and low laser intensities were used. Under these conditions, a massive oscillatory activity was observed to occur spontaneously in astrocytes (Figure

7.14B, 7.15A). In contrast to neuronal up-states, spontaneous astrocytic oscillations were not synchronous, but they exhibited a complex spatial-temporal organization. Only occasionally some degree of synchrony was observed. Simultaneous patch-clamp current-clamp recordings and Ca^{2+} imaging allowed us to detect spontaneous activities from both neurons and astrocytes. However, due to the complexity of the astrocytic oscillations, spatial-temporal relationship between astrocytic oscillations and neuronal oscillations, it would be necessary to develop an appropriate approach that could allow the analysis the astrocytic Ca^{2+} signals in more details.

7.3.2 Preliminary investigation of the role of neuron-astrocyte cross-talk in spontaneous neuronal activity

To investigate the hypothesis whether neuron-astrocyte crosstalk play a role in the generation or modulation of the spontaneous neuronal network activity, spontaneous astrocytic oscillations have been silenced by application of cyclopiazonic acid. Up-states in neurons were observed by Ca^{2+} imaging and in some experiments by simultaneous current-clamp recordings and Ca^{2+} imaging. Up-states frequency and duration have been measured before and after CPA application; to detect a statistically sufficient number of up-states a period of ten minutes has been considered for the frequency calculation. Given the matching between oscillations in the voltage of the patched neurons and in Ca^{2+} signal from other neurons, up-states frequency was easily obtainable by both of them; contrarily up-states duration has been exclusively calculated from current-clamp traces, due to their higher temporal resolution.

Current-clamp and Ca^{2+} imaging recordings up to thirty minutes without CPA application were taken as a control of the up-states frequency stability during long recordings. CPA application selectively suppressed spontaneous astrocytic oscillations after about twenty minutes (Figure 7.15A). After ten minutes of CPA application up-states frequency was significantly decreased to 73 ± 6% of control frequency ($n = 6$, $p = 0.007$) in WT mice; after twenty minutes of CPA application up-states frequency was decreased to 59 ± 3% of control frequency ($n = 6$, $p = 0.0001$) (Figure 5.16B, 5.16C).

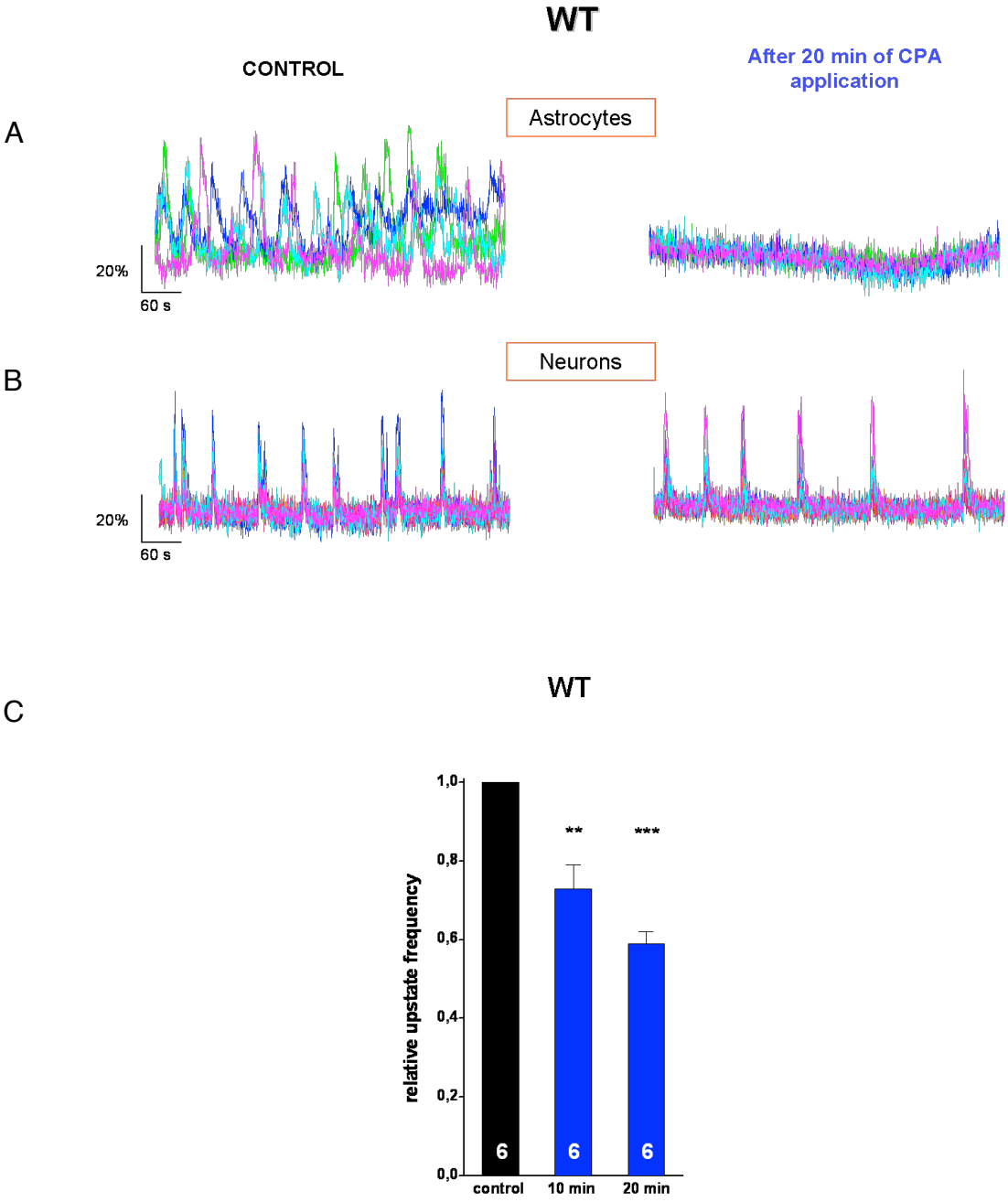

Figure 7.15: CPA (50 µM) application suppresses astrocytic spontaneous activity and reduces neuronal up-states frequency in WT mice

A: Ca^{2+} traces from representative astrocytes from WT brain slices before (control) and after CPA application. CPA have the same effect on KI astrocytes (not shown).

B: Ca^{2+} traces from representative neurons from WT brain slices before and after CPA application.

C: Average relative up-state frequency before (control) and after CPA application for 10 and 20 minutes. Up-state frequency has been calculated in an interval of 10 minutes; relative frequency is the ratio between observed frequency (i.e. control, 10 min CPA, and 20 min CPA) and control frequency. n = 6 experiments from WT mice brain slices

After ten minutes of CPA application up-states frequency was almost unaltered (97 ± 3% n = 4, p = 0.40) in KI mice; after twenty minutes of CPA application up-states frequency was decreased to 89 ± 6% of control frequency (n = 4, p = 0.12) (Figure

7.16A, 7.16B). Up-states duration in WT before and after CPA application were not significantly different (relative duration in the presence of CPA was 1.06 ± 0.02, n = 3, p = 0.09).

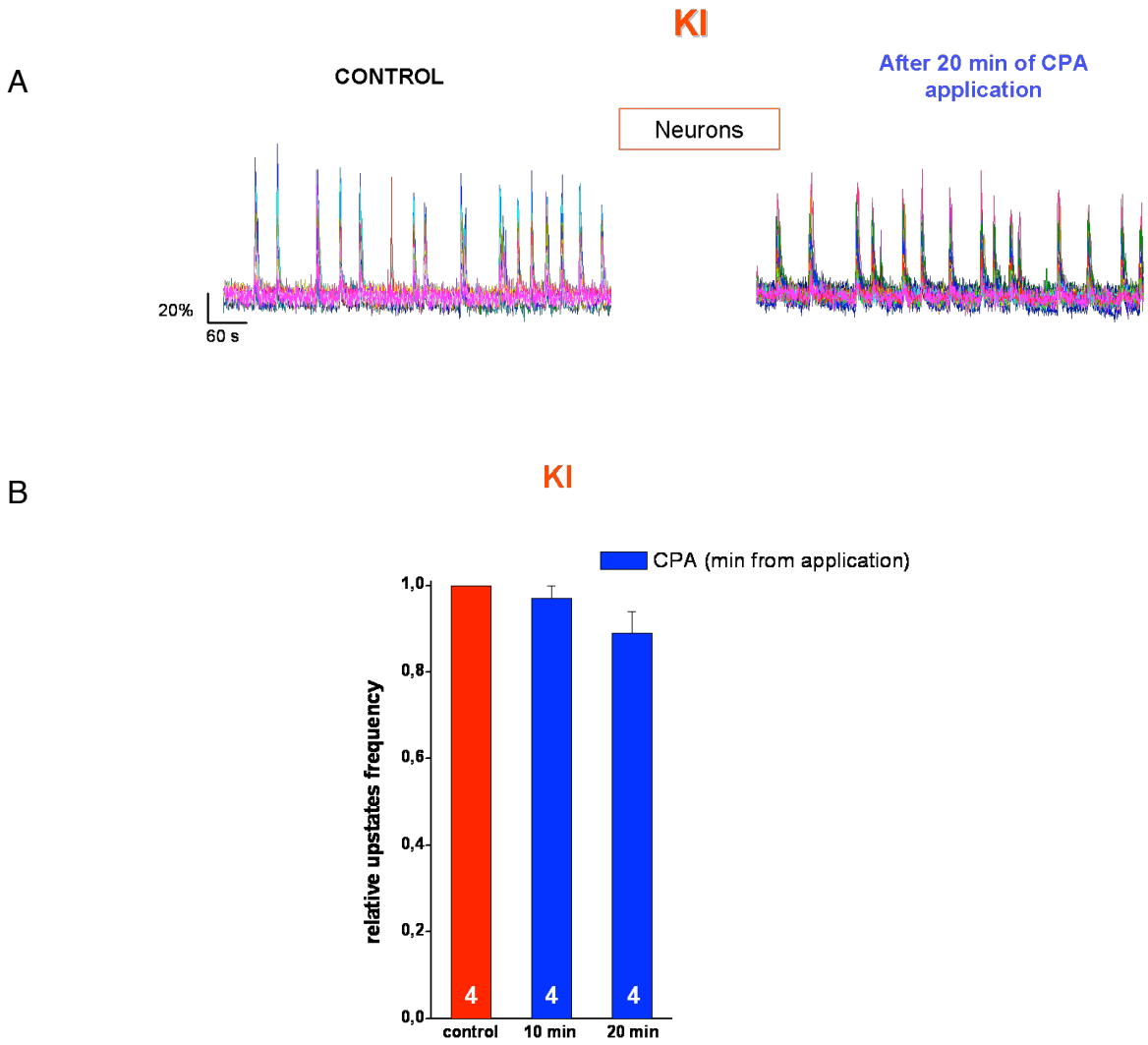

Figure 7.16: CPA (50 µM) application does not significantly reduces neuronal up-states frequency in R192Q KI mice

A: Ca^{2+} traces from representative neurons from RQ brain slices before and after CPA application.

B: Average relative up-state frequency before (control) and after CPA application for 10 and 20 minutes Up-state frequency has been calculated in an interval of 10 minutes; relative frequency is the ratio between observed frequency (i.e. control, 10 min CPA, and 20 min CPA) and control frequency.. n = 4 experiments from RQ mice brain slices.

8. Discussion (II)

Findings of Tottene et al. (2009) and results reported in chapter 3 are in agreement with and support a model of experimental CSD induction triggered by a feed-forward cycle of increasing $[K^+]_{out}$/neuronal depolarization that becomes self-regenerating when sufficient strong stimuli are applied. Moreover, findings published in Tottene et al. (2011) demonstrated the necessary role of presynaptic (and possibly postsynaptic) P/Q-type Ca^{2+} channels and of NMDA receptors in WT mice. In striking contrast preliminary evidences from FHM1 RQ KI mice may suggest that some other elements may participate in CSD induction and propagation.

CSD was induced by high KCl pressure pulses of increasing duration (at the fixed pressure of 0.5 bar), given at 5 minutes intervals with an increase step of 20 ms. When stimuli such intense to ignite a CSD were applied, a strong change in IOS, spreading on the slice surface was detected; beside this, a typical depolarization to almost 0 mV was recorded in a pyramidal cell located 600 μm afar from the pressure-injecting pipette tip. No voltage changes could be detected after sub-threshold KCl stimuli at this distance. Notably, sub-threshold stimuli produce non propagating circular IOS changes, with a radius up to about 150 μm. To investigate in detail the mechanisms of CSD induction and propagation, patch clamp recording were made at 100 and 200 μm from KCl-injecting pipette, where it was possible to record both CSD and membrane depolarizations induced by sub-threshold KCl stimuli. Layer 2/3 pyramidal cells located 100 μm from the KCl were in fact very close to the KCl injection site and indeed they were often located within the circular area interested in IOS changes; pyramidal neurons at 200 μm were also close to KCl-injecting pipette, but out from the area covered by non propagating light transmittance changes. In current-clamp recordings from cell located at 100 μm it has been possible to distinguish three peaks: two peaks characterizing sub-threshold stimuli and a CSD-specific one. Low intensity stimuli produced only a rapid depolarization with firing, ending in a noisy peak; higher intensity stimuli led depolarizations also characterized by a the same rapid phase and the first noisy peak, with an additional second, less noisy and peak. The intensity of the both the first and the second peak varied as a function of the intensity of the KCl pulse; however, the first peak was always smaller in amplitude than the second one, that, indeed, reached often a voltage close to 0 mV. When stimuli so intense to ignite a CSD were applied it was possible to record an additional third peak, whose amplitude was similar to the second one. At the distance of 200 μm after a sub-threshold pulse it was also possible to detect the first and the second peaks, but they were smaller in amplitude and slower in kinetics; moreover at distance it was often difficult to separate them,

because of their partial overlapping. Also in this case a CSD produced a third peak that was never detectable after sub-threshold pulses.

Patch-clamp recordings allowed a very accurate description of sub-threshold depolarizations and of CSD, with low noise and a high temporal resolution. Patch-clamp recordings were, however, restricted to one neuron. In contrast, Ca^{2+} imaging, in spite of the less accuracy and the smaller temporal resolution, allowed to monitor the activity from several neurons at the same time. In fact Ca^{2+} imaging did not provide additional informations on the kinetic of CSD phases; this technique allowed, instead, to observe the spatial characteristics of CSD induction and propagation. Fluorescence signals from tens of neurons at different distances from the KCl-injection pipette tip were scanned at the same time for each KCl pulse. Ca^{2+} imaging experiments confirmed observations obtained from patched cells, allowing to detect, after each sub-threshold stimulus, a neuronal Ca^{2+} peak whose amplitude decreased as a function of the distance from the KCl-injection site, until no signal was detectable in distant neurons. The amplitude of Ca^{2+} peaks and the spatial recruitment of neurons increased with increasing pulse intensity, until all neurons in the observation field were activated by the propagating CSD. CSD induced the appearance of a second peak in Ca^{2+} traces: contrarily to sub-threshold peaks, the CSD-linked additional peak did not vary with distance from KCl-injection site. Given the higher time frame (491 ms with 7 line averaging) of confocal acquisitions compared to patch clamp recordings, sub-threshold Ca^{2+} traces showed only one peak, instead of the two observed by current-clamp. Simultaneous patch clamp and Ca^{2+} imaging experiments showed a general correlations between voltage changes and Ca^{2+} increases at the same distance: in particular the first and the second fluorescence peak respectively corresponded to the second and the third voltage peak.

A overall view of the different phases detectable after both sub-threshold and threshold KCl stimuli clearly indicates the real complexity of the CSD. KCl stimuli of increasing intensity induced, indeed, multi-phase neuronal depolarizations with firing of in an increasing neuronal population; moreover, the amplitude and the kinetics of these depolarizations vary with pulse intensity and with distance. The only difference I found between depolarizations induced by stimuli that failed to induce a CSD, and a propagating CSD, is the appearance of a specific CSD-linked peak, detectable by both current-clamp and Ca^{2+} imaging in all observed neurons. Currently, it is very difficult to understand the physiological meanings of the different CSD phases and their importance in determining the appearance of the specific CSD-linked propagating peak. A possible interpretation of the rapid depolarization with firing that precedes the first voltage peak may be the summation of the post-synaptic potentials (PSPs) due to the progressive activation of neurons connected with the patched one. The first voltage peak

may be due, instead, to the direct effect of K^+ on the neuron. Further experiments will have the aim of pharmacological dissection of the different voltage phases and of determining their relevance in inducing CSD.

Ca^{2+} imaging experiments allowed to observe also astrocytic Ca^{2+} increases induced by KCl stimuli used to induce CSD. Astrocytes could be recognize on the basis on their small dimension and greater fluorescence emission; beside, to confirm these morphological criteria, some slices were double loaded with both a Ca^{2+}-sensitive indicator and the specific astrocytic dye SR101, allowing to finely distinguish neurons and astrocytes. Increasing KCl pulses activated an increasing number of astrocytes in the observation field, until almost all were recruited during CSD. Astrocytic response to KCl were very different from an astrocyte to another and often presented a variable number of additional Ca^{2+} oscillations after the first response to KCl.

Given the well established glutamatergic intercommunication between neurons and astrocytes and the fact that astrocytic glutamate release acts specifically on NMDA receptors I investigated whether astrocytes can contribute to CSD induction and propagation. The working hypothesis was that astrocytic glutamate release, triggered by neuronal activation, contributed to determine CSD induction threshold, especially in RQ mice, which show an increased glutamate release from pyramidal neurons. To check this hypothesis I decided to measure CSD threshold and velocity, using the same well established protocol presented above, before and after suppression of astrocytic gliotransmission. Astrocytic gliotransmitter release is mediated by increases in $[Ca]_{int}$, that are, in turn, mediated by the activation of several astrocytic receptors for neurotransmitters. Different pharmacological tool can be used for silencing astrocytic signaling; the most specific one is patch-perfusion of astrocytic syncytium with a Ca^{2+} chelator (i.e BAPTA), however it can affect only a small area in a brain slice. The most suited tool was slice perfusion with a compound able to suppress $[Ca^{2+}]_{int}$ elevation in astrocytes without affecting neuronal activity. Cyclopiazonic acid (CPA), a SERCA inhibitor, was able to empty astrocytic Ca^{2+} intracellular stores, thus preventing astrocytic Ca^{2+} elevations without affecting neuronal responses to KCl stimuli. In spite of this, application of CPA did not affect CSD threshold or velocity in both WT and KI mice, where a major effect of astrocytes was expected. This evidence does not contradict the existence or the importance of neuron-astrocyte cross-talk, but excludes the possibility that this mechanisms can play a role in experimental CSD induction, at least in our in vitro model.

In spite of the evidence that neuron-astrocytes crosstalk is not involved in CSD induction and propagation mechanisms, preliminary evidences that could agree with a role of astrocytes in neuronal cortical spontaneous activity have been provided. During Ca^{2+} imaging experiments in some slices it was possible to observe spontaneous

oscillations which occurred synchronously in a large amount of neurons with a frequency of about 2 events per minute; moreover these oscillations occurred at the same time in both neurons that responded to KCl stimuli and other neurons. Simultaneous patch clamp and Ca^{2+} imaging experiments showed a remarked correspondence between these Ca^{2+} oscillations and the well known, but not yet well characterized, spontaneous voltage oscillations between up- and down-states that can be observed in particular conditions in brain slices with current-clamp recordings. In addition Ca^{2+} imaging allowed to observe slow spontaneous Ca^{2+} oscillations from several astrocytes in the observation field. Recent findings demonstrated that high power laser observations can alter spontaneous astrocytic activity in vivo (Kuga et al., 2011). To minimize the influence of laser power in Ca^{2+} imaging observation I adopted a low laser power protocol for confocal observation: slices were indeed loaded with the Ca^{2+}-sensitive indicator Fluo-4, which have a wider dynamic range than OGB1-AM, and laser power was set at a very low intensity, allowing to distinguish finely distinguish only astrocytes and active neurons. This protocol allowed to observe and acquire Ca^{2+} signals for up to tens on minutes, thus observing a high number of spontaneous oscillations in both neurons and astrocytes. A wide amount of astrocytes showed large Ca^{2+} rises that occurred with different kinetics and different periods in different astrocytes: in some astrocytes, indeed, this activity was continue, with an almost fixed period, while in others only one or two sporadic rises were detect in a time series of 10 minutes. While neuronal up-states are very synchronous, astrocytic oscillations showed no clear spatial or temporal correlation. In spite of this, some synchronicity (not shown) can be found in some astrocytes. Further correlation analyses will be performed using a dedicated MATLAB algorithm, that I am presently developing. CPA application for 20 minutes completely suppressed astrocytic spontaneous activity in both WT and R192Q KI mice, but yielded to different effects on the two strain of mice. In WT CPA application significantly reduced up-states frequency of about the 40%, while in KI mice it produced only a small, not significant effect. These findings clearly indicate that application of CPA can influence spontaneous cortical network activity and are in agreement with a possible role of astrocytes in the generation of modulation of up-states. In spite of this, no convincing direct evidence of a similar role have been provided yet. Further experiments will try to investigate whether CPA exert direct effect or not on neuronal synaptic activity. Moreover different protocol for inhibit or stimulate astrocytes will be tried.

9. Materials and methods

9.1 Animals

All the experiments have been performed on brain slices from WT C57Bl/6J mice (genetic background: 87.5%) and the corresponding homozygous KI mice carrying the $Ca_V2.1$ R192Q FHM1 mutation as described in van den Maagdenberg et al. (2004) and in van den Maagdenberg et al. (2010). These strain are distributed by The Jackson laboratories.

Experiments have been performed on brain slices from mice from postnatal day 15 to 18.

All experimental procedures were carried out in accordance with the Italian Animal Welfare Act and approved by the local authority veterinary service.

9.2 Coronal cortical slices preparation

9.2.1 Solutions

Standard Artificial Cerebrospinal Fluid (sACSF*)*: NaCl 125 mM, KCl 2.5 mM, $MgCl_2$ 1 mM, $CaCl_2$ 2 mM, $NaHCO_3$ 25 mM, NaH_2PO_4 1.25 mM, glucose 25 mM, minocycline 50 nM, saturated with 95% O_2 and 5% CO_2 (pH 7.4 with NaOH).

Gluconate Cutting Solution (GCS): KGluconate 130 mM, KCl 15 mM, EGTA 0.2 mM, HEPES 20 mM, glucose 25 mM, kynurenic acid 2 mM, minocycline 50 nM saturated with 100% O_2 (pH 7.4).

Mannitol Cutting Solution (MCS): D-mannitol 225 mM, glucose 25 mM, KCl 2.5 mM, NaH_2PO_4 1.25 mM, $NaHCO_3$ 26 mM, $CaCl_2$ 0.8 mM, $MgCl_2$ 8 mM, kynurenic acid 2 mM, minocycline 50 nM, saturated with 95% O_2 and 5% CO_2 (pH 7.4).

GCS, MCS e sACSF contain minocycline (SIGMA M9511), a microglia inhibitor, to prevent immune responses. GCS and MCS contain kinurenic acid (Tocris 0223), a NMDA receptor blocker, to prevent excitotoxicity during slices cutting.

9.2.2 Slices preparation

Slice cutting protocol adopted in my laboratory has been developed by Dr Stephane Dieudonné (*École Normale de Paris*) and is described in Dugué et al., 2005. This protocol is characterized by the presence of the GCS, that mimics the intracellular ionic composition to enhance the recovery of neurons after cutting; moreover 0 mM Ca^{2+} in GCS prevents neuronal activity, thus preventing excitotoxicity.

Mice were anesthetized with isofluorane and decapitated; the whole head was immediately put into ice-cold ACSF, where the scalp was removed and the skull opened. The brain was quickly removed and put in fresh ice-cold ACSF. Cerebellum was removed by a cut in the coronal (frontal) plane, creating also a basis surface for fixing with commercial glue the brain to the slicer support.

Acute 350 μm thick coronal slices were cut in ice-cold GCS with a vibratome (Leica VT1000S); left and right hemispheres were separated. Slices putatively containing the barrel cortex were selected and then transferred at room temperature for 1 minute in MCS. This solution present a ionic composition intermediate between GCS and sACSF and allowed an intermediate recovery passage for slices before being transferred in sACSF. Slices were indeed maintained in sACSF at 30 °C for 30 minutes and finally at room temperature for 30 minutes, allowing neurons recovering after the sectioning procedures. Each slice was maintained for at least 20 minutes in recording solution before electrophysiological recordings started.

All the experiments were performed within 6 hours from the decapitation of the animal.

9.3 Patch clamp technique

The basis for patch clamp technique is to isolate electrically a membrane patch from the extracellular solution using a thin glass pipette touching the surface of the cell and applying a negative pressure. A correct patch clamp procedure allows the formation of an high resistance seal (in the order of GΩ) between the cellular membrane and the pipette tip. To avoid the contact of the tip with eventual impurities present in the bath solution, that may hinder the formation of a good seal, a positive pressure must be applied while the pipette is in bath; moreover this step become fundamental while the pipette penetrates and progresses into brain tissue, until it reaches the chosen cell.

The pipette, filled with a suitable solution that mimics the cytosol composition, contains a silver electrode covered with silver chloride; this is connected to a feedback amplification system (patch amplifier). The amplifier allows to control the voltage difference across the membrane, detecting the difference between the membrane potential and the potential set by the operator and injecting a current of opposite sign (voltage-clamp); the same electrical circuit allows current measurements while the membrane potential is controlled. Alternatively the same amplification system allows to measure membrane potential variations after injections of amounts of current (even null) set by the operator (current-clamp).

After establishment of a good and stable seal four different configurations can be obtained:

1) cell-attached: the membrane patch is conserved and not broken. This configuration allows measurements of single channel current (if a channel or more are present in the patch) without altering cytosol;

2) inside-out: is obtained from cell-attached configuration by withdrawing the pipette from the cell. The intracellular surface of the membrane patch faces the bath solution;

3) whole-cell: the membrane patch is broken by application of brief pulses of negative pressure, causing the pipette solution diffusion in the cytoplasm. This configuration allows the measurement of the current flowing through all the channels expressed in the plasma membrane or of the voltage changes of the whole cell;

d) outside-out: is obtained from whole-cell configuration by withdrawing the pipette tip. The intracellular surface of the patch faces the solution contained in the pipette.

9.4 Patch clamp setups and recordings

During experiments brain slices were maintained in a chamber and continuously perfused with fresh extracellular solution saturated with 95% O_2 and 5% CO_2 at 3 ml/ min.

Recordings of CSD and spontaneous activity were performed on layer 2/3 pyramidal cell of somatosensory cortex (barrel cortex); this cortical area was recognized by the presence of barrel-like typical structures in the layer 4 (Petersen, 2007). Recordings were made from cells at least 45 μm deep. Pyramidal cells were identified on the basis of their typical morphology (triangular soma, a main apical dendrite pointing towards the pia and the absence of a main dendrite in the opposite direction); moreover, the characteristic AP-firing induced by supra-threshold current injections of increasing amplitudes up to 400 pA in current-clamp was an additional, more specific, parameter. The firing of pyramidal cells indeed shows a typical spike frequency adaptation and the maximal frequency of firing is close to 20 Hz; the second AP in a series is wider than the first, and the development of an adaptive hump as the cell is further depolarized is generally observed.

Patch-clamp pipettes were obtained from borosilicate capillaries (Wiretrol II 5-000-2050), previously polished by fire and alcohol, using the puller P-95 (Sutter Instruments). The resistance of pipettes in the bath ranged between 3 and 5 MΩ.

All the experiments have been done in whole-cell configuration in current-clamp mode, using two different setups.

9.4.1 Solutions

Modified Artificial Cerebrospinal Fluid (mACSF, recording solution): NaCl 125 mM, KCl 3.5 mM, $MgCl_2$ 0.5 mM, $CaCl_2$ 1 mM, $NaHCO_3$ 25 mM, NaH_2PO_4 1.25 mM, glucose 25 mM. saturated with 95% O_2 e 5% CO_2 (pH 7.4).

mACSF differs from sACSF for the slightly higher K^+ concentration and lower Ca^{2+} and Mg^{2+} one. This modified solution composition is more similar to real cerebrospinal fluid composition (Chutkow, 1974; Zhang et al., 1990) and allows observation of an higher spontaneous activity compared to the standard one (Sanchez-Vives et al., 2000).

Intracellular solution: KCl 6 mM, KGluconate114 mM, HEPES 10 mM, Na phosphocreatine 10 mM, MgATP 4 mM, NaGTP 0,3 mM, (pH 7.40 with NaOH, osmolarity 300 mOsm).

9.4.2 Patch clamp setup (i)

Slices observation and patch clamp recordings were made with an upright microscope (Nikon Instruments, Eclipse E600FN) equipped with patch clamp equipment (read below); slice were observed under infrared differential interference contrast (IR DIC). Two different objectives were available: a 10X Nikon objective, for preliminary slices inspection and for IOS imaging during CSD, and a water immersion 60X Nikon objective, for the patch clamp procedures. Two CCD cameras (Hamamatsu Photonics K.K., Hitachi) were connected to the microscope for live observations and IOS optical recordings.

Electrical signals were recorded through a Multiclamp 700B patch-clamp amplifier and digitized using a Digidata 1322A interface and pClamp software (all from Molecular Devices). Signals were low-pass filtered at 2 kHz and sampled at 10 kHz. Experiments were performed at room temperature (RT).

Liquid junction potential (LJP) measured at the pipette tip was -12 mV. LJP should be added to all voltages to obtain the correct values of membrane potential in whole-cell recordings.

9.4.3 Patch clamp setup (ii)

Simultaneous Ca^{2+} imaging and patch clamp recordings were made with an upright confocal microscope (Leica, TCS-SP5-RS) equipped with patch clamp equipment (read below), a 20X objective (NA, 1.0), and a CCD camera (DFC 350FX, Leica) for IR DIC images.

Electrical signals were recorded through a Axopatch-200B patch clamp amplifier and digitized using a Digidata 1320 interface and pClamp software (all from Molecular Devices). Signals were low-pass filtered at 1 kHz and sampled at 5 kHz. Experiments were performed at room temperature (RT).

Calculated LJP was -15 mV.

A precise alignment of Ca^{2+} and electrophysiological signals was achieved by acquiring with a synchronization signal produced by the confocal microscope.

9.4.4 Data analysis

Patch-clamp experiments were analyzed using the Clampfit 10.0 software from the pClamp suite (Molecular Devices). All averages were calculated with Microsoft Excel. Graphs and statistical comparison were obtained with the Origin software (Microcal Software, Inc.). Data are given as mean ± SEM; stars indicate a statistically significant difference from control assessed by the Student's t test (*$p < 0.05$, **$p < 0.01$ and ***$p < 0.001$).

9.5 Slices loading with Ca^{2+}-sensitive indicators

Brain was quickly removed and slices cut as previously described; after hemispheres separation, subcortical structures were carefully dissected and removed to reduce the slice volume for optimizing the loading quality. Slices putatively containing the barrel cortex were selected and then transferred at room temperature for 1 minute in MCS. Slices were then transferred to sACSF at 32 °C for 15 minutes and then loaded with the Ca^{2+}-sensitive indicators Oregon Green® 488 BAPTA-1, AM (OGB1-AM, 12.5 µg/µl, Invitrogen) for 60 minutes at 32 °C or Fluo-4, AM (12.5 µg/µl, Invitrogen) for 45 minutes at 32 °C. Loading was performed in sACSF containing sulfinpyrazone (200 mM), pluronic (0.12%), and kynurenic acid (1 mM). After loading, slices were recovered and kept at room temperature in the presence of 200 mM sulfinpyrazone.

In some experiments slice were loaded with both the Ca^{2+} indicator Fluo-4 and the astrocyte-selective dye sulforhodamine 101 (SR101, 0.1 µM, Invitrogen), to specifically distinguish neurons and astrocytes (see Figure 5.7 in the Results section); in this case slices were transferred immediately after cutting in sACSF plus 0.1 µM SR101 at 32 °C for 15 minutes, before Fluo-4 loading.

9.6 Confocal microscopy and Ca^{2+} imaging

Ca^{2+} imaging experiments were made with an upright confocal microscope (Leica, TCS-SP5-RS) equipped with patch clamp equipment, a 20X objective (NA, 1.0), and a CCD camera (DFC 350FX, Leica) for IR DIC images.

Laser emission at 488 nm was used for stimulation of OGB1-AM and Fluo-4; SR101 was excited at 543 nm. Time frame acquisitions of 491 ms were used, with 7 line averaging; no background subtraction or other manipulations were applied to digitized Ca^{2+} signal images that are reported as raw data.

9.6.1 Data analysis

Ca^{2+} imaging acquisitions were analyzed using the LAS-AF (Leica), MATLAB (The MathWorks) and MBT-ImageJ softwares.

The Ca2+ signals are reported as ΔF/F0, where ΔF is the fluorescence change and F0 is the baseline fluorescence.

9.7 Experimental CSD

Brain slices were perfused with mACSF at a flowing rate of 3 ml/min, and pressure pulses of 3 M KCl (at 0.5 bar) of increasing duration (at 5 min intervals in 20 ms steps) were applied through a glass micropipette (resistance ranging from 0.19 to 0.25 MΩ) onto the slice surface on layer 2/3, using a PDES-02DX pneumatic drug ejection system (Npi Electronic), until a CSD was elicited. CSD was detected by the associated change in intrinsic optical signal (IOS) and/or recording in current-clamp the membrane potential of a pyramidal cell at 600 μm from the pressure-ejection pipette tip (See Figure 4.1). The duration of the first pulse eliciting a CSD was taken as CSD threshold and the rate of horizontal spread of the change in IOS as CSD velocity.

In control experiments, similar CSD threshold and velocity were found when two CSD episodes were induced at a 30 min interval on the same slice.

To test the effect of different toxins and drugs, CSD threshold and velocity were measured before and after 30 min of perfusion with mACSF plus saturating concentrations of the chosen drug.

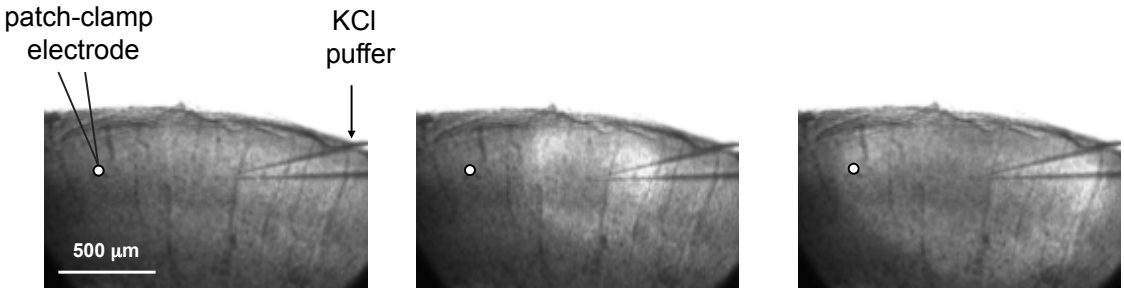

Figure 4.1: Experimental CSD induction by high KCl pressure pulses

Three different frames from a CCD acquisition showing a representative slice before (first frame) and after CSD induction. Note the patch clamp pipette (on the left side of the slice), located at 600 µm from the KCl-injecting pipette (on the right side of the slice).

10. Reference list

Amzica, F., and Steriade, M. (1995). Short- and long-range neuronal synchronization of the slow (< 1 Hz) cortical oscillation. J. Neurophysiol. 73, 20-38.

Araque, A., Parpura, V., Sanzgiri, R.P., and Haydon, P.G. (1999). Tripartite synapses: glia, the unacknowledged partner. Trends Neurosci. 22, 208-215.

Arikkath, J., and Campbell, K.P. (2003). Auxiliary subunits: essential components of the voltage-gated calcium channel complex. Curr. Opin. Neurobiol. 13, 298-307.

Ayata, C., Jin, H., Kudo, C., Dalkara, T., and Moskowitz, M.A. (2006). Suppression of cortical spreading depression in migraine prophylaxis. Ann. Neurol. 59, 652-661.

Bazhenov, M., Timofeev, I., Steriade, M., and Sejnowski, T.J. (2002). Model of thalamocortical slow-wave sleep oscillations and transitions to activated States. J. Neurosci. 22, 8691-8704.

Bezzi, P., Carmignoto, G., Pasti, L., Vesce, S., Rossi, D., Rizzini, B.L., Pozzan, T., and Volterra, A. (1998). Prostaglandins stimulate calcium-dependent glutamate release in astrocytes. Nature 391, 281-285.

Bliss, T.V., and Collingridge, G.L. (1993). A synaptic model of memory: long-term potentiation in the hippocampus. Nature 361, 31-39.

Bushong, E.A., Martone, M.E., Jones, Y.Z., and Ellisman, M.H. (2002). Protoplasmic astrocytes in CA1 stratum radiatum occupy separate anatomical domains. J. Neurosci. 22, 183-192.

Cartmell, J., and Schoepp, D.D. (2000). Regulation of neurotransmitter release by metabotropic glutamate receptors. J. Neurochem. 75, 889-907.

Castillo, P.E., Malenka, R.C., and Nicoll, R.A. (1997). Kainate receptors mediate a slow postsynaptic current in hippocampal CA3 neurons. Nature 388, 182-186.

Catterall, W.A. (2011). Voltage-gated calcium channels. Cold Spring Harb Perspect. Biol. 3, a003947.

Catterall, W.A., and Few, A.P. (2008). Calcium channel regulation and presynaptic plasticity. Neuron 59, 882-901.

Catterall, W.A., Perez-Reyes, E., Snutch, T.P., and Striessnig, J. (2005). International Union of Pharmacology. XLVIII. Nomenclature and structure-function relationships of voltage-gated calcium channels. Pharmacol. Rev. 57, 411-425.

Charles, A.C. (1994). Glia-neuron intercellular calcium signaling. Dev. Neurosci. 16, 196-206.

Chutkow, J.G. (1974). Metabolism of magnesium in central nervous system. Relationship between concentrations of magnesium in cerebrospinal fluid and brain in magnesium deficiency. Neurology 24, 780-787.

Collingridge, G.L., Olsen, R.W., Peters, J., and Spedding, M. (2009). A nomenclature for ligand-gated ion channels. Neuropharmacology 56, 2-5.

Cull-Candy, S.G., and Leszkiewicz, D.N. (2004). Role of distinct NMDA receptor subtypes at central synapses. Sci. STKE 2004, re16.

Dalkara, T., Zervas, N.T., and Moskowitz, M.A. (2006). From spreading depression to the trigeminovascular system. Neurol. Sci. 27 Suppl 2, S86-90.

Davies, A., Hendrich, J., Van Minh, A.T., Wratten, J., Douglas, L., and Dolphin, A.C. (2007). Functional biology of the alpha(2)delta subunits of voltage-gated calcium channels. Trends Pharmacol. Sci. 28, 220-228.

Dingledine, R., Borges, K., Bowie, D., and Traynelis, S.F. (1999). The glutamate receptor ion channels. Pharmacol. Rev. 51, 7-61.

Dubel, S.J., Starr, T.V., Hell, J., Ahlijanian, M.K., Enyeart, J.J., Catterall, W.A., and Snutch, T.P. (1992). Molecular cloning of the alpha-1 subunit of an omega-conotoxin-sensitive calcium channel. Proc. Natl. Acad. Sci. U. S. A. 89, 5058-5062.

Dugue, G.P., Dumoulin, A., Triller, A., and Dieudonne, S. (2005). Target-dependent use of co-released inhibitory transmitters at central synapses. J. Neurosci. 25, 6490-6498.

Ertel, E.A., Campbell, K.P., Harpold, M.M., Hofmann, F., Mori, Y., Perez-Reyes, E., Schwartz, A., Snutch, T.P., Tanabe, T., Birnbaumer, L., Tsien, R.W., and Catterall, W.A. (2000). Nomenclature of voltage-gated calcium channels. Neuron 25, 533-535.

Fellin, T., Pascual, O., Gobbo, S., Pozzan, T., Haydon, P.G., and Carmignoto, G. (2004). Neuronal synchrony mediated by astrocytic glutamate through activation of extrasynaptic NMDA receptors. Neuron 43, 729-743.

Gasparini, S., Kasyanov, A.M., Pietrobon, D., Voronin, L.L., and Cherubini, E. (2001). Presynaptic R-type calcium channels contribute to fast excitatory synaptic transmission in the rat hippocampus. J. Neurosci. 21, 8715-8721.

Giaume, C., and McCarthy, K.D. (1996). Control of gap-junctional communication in astrocytic networks. Trends Neurosci. 19, 319-325.

Gomez-Gonzalo, M., Losi, G., Chiavegato, A., Zonta, M., Cammarota, M., Brondi, M., Vetri, F., Uva, L., Pozzan, T., de Curtis, M., Ratto, G.M., and Carmignoto, G. (2010). An excitatory loop with astrocytes contributes to drive neurons to seizure threshold. PLoS Biol. 8, e1000352.

Haider, B., Duque, A., Hasenstaub, A.R., and McCormick, D.A. (2006). Neocortical network activity in vivo is generated through a dynamic balance of excitation and inhibition. J. Neurosci. 26, 4535-4545.

Halassa, M.M., Fellin, T., Takano, H., Dong, J.H., and Haydon, P.G. (2007). Synaptic islands defined by the territory of a single astrocyte. J. Neurosci. 27, 6473-6477.

Hans, M., Luvisetto, S., Williams, M.E., Spagnolo, M., Urrutia, A., Tottene, A., Brust, P.F., Johnson, E.C., Harpold, M.M., Stauderman, K.A., and Pietrobon, D. (1999). Functional consequences of mutations in the human alpha1A calcium channel subunit linked to familial hemiplegic migraine. J. Neurosci. 19, 1610-1619.

Hassinger, T.D., Atkinson, P.B., Strecker, G.J., Whalen, L.R., Dudek, F.E., Kossel, A.H., and Kater, S.B. (1995). Evidence for glutamate-mediated activation of hippocampal neurons by glial calcium waves. J. Neurobiol. 28, 159-170.

Hassinger, T.D., Guthrie, P.B., Atkinson, P.B., Bennett, M.V., and Kater, S.B. (1996). An extracellular signaling component in propagation of astrocytic calcium waves. Proc. Natl. Acad. Sci. U. S. A. 93, 13268-13273.

Haydon, P.G., and Carmignoto, G. (2006). Astrocyte control of synaptic transmission and neurovascular coupling. Physiol. Rev. 86, 1009-1031.

Heinemann, S.H., Terlau, H., Stuhmer, W., Imoto, K., and Numa, S. (1992). Calcium channel characteristics conferred on the sodium channel by single mutations. Nature 356, 441-443.

Hille, B. (2001).
Ionic channels of excitable membranes.Sutherland MA: Sinauer).

Hofmann, F., Biel, M., and Flockerzi, V. (1994). Molecular basis for Ca2+ channel diversity. Annu. Rev. Neurosci. 17, 399-418.

Kidd, F.L., and Isaac, J.T. (2001). Kinetics and activation of postsynaptic kainate receptors at thalamocortical synapses: role of glutamate clearance. J. Neurophysiol. 86, 1139-1148.

Klugbauer, N., Lacinova, L., Marais, E., Hobom, M., and Hofmann, F. (1999). Molecular diversity of the calcium channel alpha2delta subunit. J. Neurosci. 19, 684-691.

Kohr, G. (2006). NMDA receptor function: subunit composition versus spatial distribution. Cell Tissue Res. 326, 439-446.

Kuga, N., Sasaki, T., Takahara, Y., Matsuki, N., and Ikegaya, Y. (2011). Large-scale calcium waves traveling through astrocytic networks in vivo. J. Neurosci. 31, 2607-2614.

Le Bon-Jego, M., and Yuste, R. (2007). Persistently active, pacemaker-like neurons in neocortex. Front. Neurosci. 1, 123-129.

Levy, D., Moskowitz, M.A., Nuseda, R., and Burstein, R. (2011). Activation of the migraine pain pathway by cortical spreading depression: Do we need more evidence? Cephalalgia

Li, L., Bischofberger, J., and Jonas, P. (2007). Differential gating and recruitment of P/Q-, N-, and R-type Ca2+ channels in hippocampal mossy fiber boutons. J. Neurosci. 27, 13420-13429.

Mangoni, M.E., Traboulsie, A., Leoni, A.L., Couette, B., Marger, L., Le Quang, K., Kupfer, E., Cohen-Solal, A., Vilar, J., Shin, H.S., et al. (2006). Bradycardia and slowing of the atrioventricular conduction in mice lacking CaV3.1/alpha1G T-type calcium channels. Circ. Res. 98, 1422-1430.

Mintz, I.M., Sabatini, B.L., and Regehr, W.G. (1995). Calcium control of transmitter release at a cerebellar synapse. Neuron 15, 675-688.

Moldrich, R.X., Chapman, A.G., De Sarro, G., and Meldrum, B.S. (2003). Glutamate metabotropic receptors as targets for drug therapy in epilepsy. Eur. J. Pharmacol. 476, 3-16.

Monyer, H., Sprengel, R., Schoepfer, R., Herb, A., Higuchi, M., Lomeli, H., Burnashev, N., Sakmann, B., and Seeburg, P.H. (1992). Heteromeric NMDA receptors: molecular and functional distinction of subtypes. Science 256, 1217-1221.

Mori, H., and Mishina, M. (1995). Structure and function of the NMDA receptor channel. Neuropharmacology 34, 1219-1237.

Mori, Y., Friedrich, T., Kim, M.S., Mikami, A., Nakai, J., Ruth, P., Bosse, E., Hofmann, F., Flockerzi, V., and Furuichi, T. (1991). Primary structure and functional expression from complementary DNA of a brain calcium channel. Nature 350, 398-402.

Moriyoshi, K., Masu, M., Ishii, T., Shigemoto, R., Mizuno, N., and Nakanishi, S. (1991). Molecular cloning and characterization of the rat NMDA receptor. Nature 354, 31-37.

Nedergaard, M. (1994). Direct signaling from astrocytes to neurons in cultures of mammalian brain cells. Science 263, 1768-1771.

Paoletti, P. (2011). Molecular basis of NMDA receptor functional diversity. Eur. J. Neurosci. 33, 1351-1365.

Parpura, V., Basarsky, T.A., Liu, F., Jeftinija, K., Jeftinija, S., and Haydon, P.G. (1994). Glutamate-mediated astrocyte-neuron signalling. Nature 369, 744-747.

Pasti, L., Volterra, A., Pozzan, T., and Carmignoto, G. (1997). Intracellular calcium oscillations in astrocytes: a highly plastic, bidirectional form of communication between neurons and astrocytes in situ. J. Neurosci. 17, 7817-7830.

Perez-Reyes, E. (2003). Molecular physiology of low-voltage-activated t-type calcium channels. Physiol. Rev. 83, 117-161.

Perez-Reyes, E., Cribbs, L.L., Daud, A., Lacerda, A.E., Barclay, J., Williamson, M.P., Fox, M., Rees, M., and Lee, J.H. (1998). Molecular characterization of a neuronal low-voltage-activated T-type calcium channel. Nature 391, 896-900.

Petersen, C.C. (2007). The functional organization of the barrel cortex. Neuron 56, 339-355.

Pietrobon, D. (2010). CaV2.1 channelopathies. Pflugers Arch. 460, 375-393.

Pietrobon, D. (2007). Familial hemiplegic migraine. Neurotherapeutics 4, 274-284.

Pietrobon, D. (2005). Migraine: new molecular mechanisms. Neuroscientist 11, 373-386.

Pietrobon, D., and Striessnig, J. (2003). Neurobiology of migraine. Nat. Rev. Neurosci. 4, 386-398.

Qian, J., and Noebels, J.L. (2001). Presynaptic Ca2+ channels and neurotransmitter release at the terminal of a mouse cortical neuron. J. Neurosci. 21, 3721-3728.

Rodriguez-Moreno, A., and Lerma, J. (1998). Kainate receptor modulation of GABA release involves a metabotropic function. Neuron 20, 1211-1218.

Sanchez-Vives, M.V., and McCormick, D.A. (2000). Cellular and network mechanisms of rhythmic recurrent activity in neocortex. Nat. Neurosci. 3, 1027-1034.

Schoepp, D.D. (2001). Unveiling the functions of presynaptic metabotropic glutamate receptors in the central nervous system. J. Pharmacol. Exp. Ther. 299, 12-20.

Seifert, G., Schilling, K., and Steinhauser, C. (2006). Astrocyte dysfunction in neurological disorders: a molecular perspective. Nat. Rev. Neurosci. 7, 194-206.

Shu, Y., Hasenstaub, A., Badoual, M., Bal, T., and McCormick, D.A. (2003). Barrages of synaptic activity control the gain and sensitivity of cortical neurons. J. Neurosci. 23, 10388-10401.

Snutch, T.P., and Reiner, P.B. (1992). Ca2+ channels: diversity of form and function. Curr. Opin. Neurobiol. 2, 247-253.

Somjen, G.G. (2001). Mechanisms of spreading depression and hypoxic spreading depression-like depolarization. Physiol. Rev. 81, 1065-1096.

Soong, T.W., Stea, A., Hodson, C.D., Dubel, S.J., Vincent, S.R., and Snutch, T.P. (1993). Structure and functional expression of a member of the low voltage-activated calcium channel family. Science 260, 1133-1136.

Starr, T.V., Prystay, W., and Snutch, T.P. (1991). Primary structure of a calcium channel that is highly expressed in the rat cerebellum. Proc. Natl. Acad. Sci. U. S. A. 88, 5621-5625.

Steriade, M., Nunez, A., and Amzica, F. (1993). A novel slow (< 1 Hz) oscillation of neocortical neurons in vivo: depolarizing and hyperpolarizing components. J. Neurosci. 13, 3252-3265.

Stern-Bach, Y., Bettler, B., Hartley, M., Sheppard, P.O., O'Hara, P.J., and Heinemann, S.F. (1994). Agonist selectivity of glutamate receptors is specified by two domains structurally related to bacterial amino acid-binding proteins. Neuron 13, 1345-1357.

Tottene, A., Conti, R., Fabbro, A., Vecchia, D., Shapovalova, M., Santello, M., van den Maagdenberg, A.M., Ferrari, M.D., and Pietrobon, D. (2009). Enhanced excitatory transmission at cortical synapses as the basis for facilitated spreading depression in Ca(v)2.1 knockin migraine mice. Neuron 61, 762-773.

Tottene, A., Fellin, T., Pagnutti, S., Luvisetto, S., Striessnig, J., Fletcher, C., and Pietrobon, D. (2002). Familial hemiplegic migraine mutations increase Ca(2+) influx through single human CaV2.1 channels and decrease maximal CaV2.1 current density in neurons. Proc. Natl. Acad. Sci. U. S. A. 99, 13284-13289.

Tottene, A., Pivotto, F., Fellin, T., Cesetti, T., van den Maagdenberg, A.M., and Pietrobon, D. (2005). Specific kinetic alterations of human CaV2.1 calcium channels produced by mutation S218L causing familial hemiplegic migraine and delayed cerebral edema and coma after minor head trauma. J. Biol. Chem. 280, 17678-17686.

Tottene, A., Urbani, A., and Pietrobon, D. (2011). Role of different voltage-gated Ca2+ channels in cortical spreading depression: specific requirement of P/Q-type Ca2+ channels. Channels (Austin) 5, 110-114.

Traynelis, S.F., Wollmuth, L.P., McBain, C.J., Menniti, F.S., Vance, K.M., Ogden, K.K., Hansen, K.B., Yuan, H., Myers, S.J., and Dingledine, R. (2010). Glutamate receptor ion channels: structure, regulation, and function. Pharmacol. Rev. 62, 405-496.

van den Maagdenberg, A.M., Pietrobon, D., Pizzorusso, T., Kaja, S., Broos, L.A., Cesetti, T., van de Ven, R.C., Tottene, A., van der Kaa, J., Plomp, J.J., Frants, R.R., and Ferrari, M.D. (2004). A Cacna1a knockin migraine mouse model with increased susceptibility to cortical spreading depression. Neuron 41, 701-710.

van den Maagdenberg, A.M., Pizzorusso, T., Kaja, S., Terpolilli, N., Shapovalova, M., Hoebeek, F.E., Barrett, C.F., Gherardini, L., van de Ven, R.C., Todorov, B., et al. (2010). High cortical spreading depression susceptibility and migraine-associated symptoms in Ca(v)2.1 S218L mice. Ann. Neurol. 67, 85-98.

Wee, K.S., Zhang, Y., Khanna, S., and Low, C.M. (2008). Immunolocalization of NMDA receptor subunit NR3B in selected structures in the rat forebrain, cerebellum, and lumbar spinal cord. J. Comp. Neurol. 509, 118-135.

Welsby, P.J., Wang, H., Wolfe, J.T., Colbran, R.J., Johnson, M.L., and Barrett, P.Q. (2003). A mechanism for the direct regulation of T-type calcium channels by Ca2+/ calmodulin-dependent kinase II. J. Neurosci. 23, 10116-10121.

Williams, M.E., Brust, P.F., Feldman, D.H., Patthi, S., Simerson, S., Maroufi, A., McCue, A.F., Velicelebi, G., Ellis, S.B., and Harpold, M.M. (1992). Structure and functional expression of an omega-conotoxin-sensitive human N-type calcium channel. Science 257, 389-395.

Wollmuth, L.P., and Sobolevsky, A.I. (2004). Structure and gating of the glutamate receptor ion channel. Trends Neurosci. 27, 321-328.

Woolf, C.J., and Salter, M.W. (2000). Neuronal plasticity: increasing the gain in pain. Science 288, 1765-1769.

Wu, L.G., Westenbroek, R.E., Borst, J.G., Catterall, W.A., and Sakmann, B. (1999). Calcium channel types with distinct presynaptic localization couple differentially to transmitter release in single calyx-type synapses. J. Neurosci. 19, 726-736.

Yu, F.H., Yarov-Yarovoy, V., Gutman, G.A., and Catterall, W.A. (2005). Overview of molecular relationships in the voltage-gated ion channel superfamily. Pharmacol. Rev. 57, 387-395.

Zhang, E.T., Hansen, A.J., Wieloch, T., and Lauritzen, M. (1990). Influence of MK-801 on brain extracellular calcium and potassium activities in severe hypoglycemia. J. Cereb. Blood Flow Metab. 10, 136-139.